

CSU/NOAA-WPL FIRE II – ASTEX FIELD EXPERIMENT DESCRIPTION OF FIELD DEPLOYMENT PHASE

by

S. Cox, C. Cornwall, W. Cotton, J. Davis, J. Kleist, T. McKee, Q. Shao,
D. Randall, W. Schubert, D. Wood

Department of Atmospheric Science

Colorado State University

Fort Collins, CO 80523

S. Frisch, M. Hardesty, R. Krophli,

J. Snider

NOAA/ERL/WPL

325 Broadway

Boulder, CO 80303

P. Anikin

Russian Academy of Science

Institute of Atmospheric Physics

Moscow, Pyzhevsky, 3

Russia

Sponsoring Agencies:

Office of Naval Research

National Aeronautics & Space Administration

National Oceanic and Atmospheric Administration

Department of Energy

The National Science Foundation



Department of Atmospheric Science

Paper No. 523

CSU/NOAA-WPL FIRE II - ASTEX FIELD EXPERIMENT

DESCRIPTION OF FIELD DEPLOYMENT PHASE

**S. Cox, C. Cornwall, W. Cotton, J. Davis, J. Kleist,
T. McKee, Q. Shao, D. Randall, W. Schubert, D. Wood**

Department of Atmospheric Science
Colorado State University
Fort Collins, CO 80523

S. Frisch, M. Hardesty, R. Kropfli, J. Snider

NOAA/ERL/WPL
325 Broadway
Boulder, CO 80303

P. Anikin

Russian Academy of Science
Institute of Atmospheric Physics
Moscow, Pyzhevsky, 3
Russia

April 1993

Atmospheric Science Paper No. 523

TABLE OF CONTENTS

1.0	Introduction	1
2.0	Surface Meteorology	11
2.1	Campbell Surface Station	11
2.2	Temperature and Relative Humidity	11
2.3	Wind Direction and Speed	13
3.0	Infrared Radiation	14
3.1	Pyrgeometer	14
3.2	PRT-6 Infrared Radiometer	16
3.3	Infrared Interferometer	21
4.0	Solar Radiation	27
4.1	Pyranometer	27
4.2	Pyrheliometer	28
4.3	Multi Field of View Radiometer (MFOV)	30
4.4	Sun Photometer	32
5.0	Upper Air	36
5.1	Radiosonde system	36
5.2	Model 400 Wind Profiler	52
5.3	Radio Acoustic Sounding System	60
6.0	Cloud Measurements	64
6.1	Laser Ceilometer	64
6.2	Video All Sky Camera	67
7.0	The NOAA/WPL Doppler K_a -Band Cloud Radar	69
8.0	NOAA/WPL Compact Doppler Lidar	71
9.0	NOAA/WPL Radiometers - Porto Santo	73
10.0	Acknowledgements	75
11.0	List of Appendices	77

LIST OF FIGURES

Figure 1:	Map of the island of Porto Santo	2
Figure 2:	Map of the locations of CSU deployment sites	3
Figure 3:	Surface Instrumentation	11
Figure 4:	Surface irradiance sensors	14
Figure 5:	PRT-6 infrared radiometer (11 micrometers)	16
Figure 6:	PRT-6 spectral response curve	17
Figure 7:	Calibration curve.	20
Figure 8:	Infrared interferometer and calibration system	21
Figure 9:	Schematic of the optical path of the dual port interferometer system	22
Figure 10a:	Example of a clear sky infrared spectrum observed	25
Figure 10b:	Example of an infrared spectrum observed in the presence of cirrus clouds	26
Figure 11:	Filtered and unfiltered pyrheliometer (see also figure 3, section 2.2)	28
Figure 12:	MFOV Radiometer	30
Figure 13:	Tracking Sun Photometer	32
Figure 14:	John Kleist (left) and William Cotton prepare for launch under windy, stratocumulus conditions on Porto Santo. Between them is the automatically tracking radiotheodolite, which measures azimuth and elevation angles of the balloon	37
Figure 15:	AIR Intellisonde, which is 10cm on the sides, 15cm high, and has a mass of 240g. The rod thermistor is on the right. The hygristor is in the radiation shielded compartment at the top of the sonde. As the sonde rises, air enters the inlet at the top, flows horizontally across the hygristor, and the exits downward at the left of the sonde. The sonde transmits at 1680 MHz via a quarter wave antenna which extends from the bottom (not visible).	38

Figure 16:	Monotone spectral response of the filter used in sections 5.11 and 5.12 for the processing of the thermodynamic and wind data. The lower abscissa is labeled in frequency (where $f = 1/2$ corresponds to one-half oscillation per data point) and the upper abscissa in period (seconds) assuming a 3 second interval between data points. The filter effectively removes oscillations with periods shorter than 18 seconds.	43
Figure 17:	The left diagram shows the balloon position (dashed vector) at azimuth α . The wind at this balloon position is v , which has horizontal components v_r in the radial direction and v_α in the tangential direction. The right diagram is a vertical plane through the center of the earth (C), the radiotheodolite observation site (O) and the balloon position (B) (after Clem et al. 1954). Here $z - z_s$ is height of the balloon above the observation site, ϵ the elevation angle, ϕ the angle subtended at the center of the earth, a the radius of the earth (assumed spherical), D the great circle distance along AB (which is concentric with OS), d the horizontal distance to the position of the balloon projected onto the tangent plane OP.	49
Figure 18:	Wind profiler system	52
Figure 19:	Wind profiler spectrum	53
Figure 20:	Ten minute wind profile	54
Figure 21:	Hourly averaged wind profile	55
Figure 22:	Sample RASS spectra (colder temperatures to the right)	63
Figure 23:	A plot of a sample histogram	66
Figure 24:	Video all sky camera convex mirror	67
Figure 25:	K_α Band Antenna Picture for ASTEX	69
Figure 26:	NOAA/WPL Doppler Lidar	72
Figure 27:	NOAA/WPL Doppler Lidar	72
Figure 28:	NOAA/ERL Microwave Radiometer	74

LIST OF TABLES

Table 1:	Surface Meteorology Observations	4
Table 2:	Infrared Radiation Observations	5
Table 3:	Solar Radiation Observations	6
Table 4:	Cloud Observations	7
Table 5:	Upper Air Observations	8
Table 6:	Summary of CSU ASTEX Data	9
Table 7:	Format of the PRT-6 data recorded in the datalogger.	18
Table 8:	Technical specifications of the MAINZ MZ II - 85 sunphotometer . . .	34
Table 9:	Dates and times (UTC) of data collected by the Mainz Sun photometer	35
Table 10:	Sample of Level I data for 2 June 0848 UTC	40
Table 11:	List of the operator selected parameters which determine the operating characteristics of the wind profiler	57
Table 12:	ASTEX Video Tapes	68
Table 13:	Characteristics of the NOAA/WPL K-Band Radar During ASTEX . . .	70
Table 14:	Specifications for the WPL Microwave 2 Channel Radiometer	73
Table 15:	Data Products Derived from WPL Radiometer Measurements	73

1.0 Introduction

During the month of June, 1992 scientists from the CSU Department of Atmospheric Science and NOAA's Wave Propagation Laboratory deployed a comprehensive set of instrumentation to monitor the marine boundary layer on the island of Porto Santo, Madeiras (33° 5' 2" N latitude and 16° 20' 49" W longitude, elevation 97m above MSL). This deployment was part of the ASTEX in which Porto Santo represented the southeast corner of a triangle constituted by the island Santa Maria in the Azores and the US research ship Malcolm Baldrige.

The experiment site was located on the north edge of the island, set back approximately 200 meters from a 100 meter cliff leading to the water's edge. The site was on airport property directly east of the north end of a 3500 meter runway. Due to a gentle slope from north to south and the fact that the site was in a small bowl, the ocean surface was generally not visible from the site location. Figure 1 presents a map of the island of Porto Santo and the relative layout of the main experimental components at the north end of the Porto Santo runway is shown in Figure 2.

The primary elements of the CSU Porto Santo observations included surface meteorology, infrared radiation, solar radiation, upper air and cloud measurements. In addition, the following instrumentation were deployed by scientists from the Wave Propagation Laboratory, ERL, NOAA: infrared doppler lidar, 8.66 mm doppler radar, solar, infrared and microwave passive radiometers. Tables 1-5 list the instrumentation deployed at the Porto Santo site by the CSU and NOAA contingents.

The experiment site was maintained twenty-four hours a day during the entire IFO (Intensive Field Observations) (6/1/92 - 6/28/92). Some remote sensing, surface radiation systems and surface meteorology systems operated continuously. Other systems operated "on demand" and data were collected only during periods of high interest. Rawinsondes were released every three hours from June 8 to June 27. From June 1 to June 8 a shortage of helium and hydrogen compressed gas dictated scaling down the rawinsonde schedule to six launches per day. Liquid nitrogen was not available on Porto Santo until June 4; therefore CSU's infrared interferometer and NOAA's doppler lidar systems operated only for the period June 4-June 27. Table 6 presents a summary of data acquired from the CSU systems during this period.

The text which follows in this document borrows heavily upon information first presented by Cox, et al., (1992) which reported Colorado State University's contribution to the FIRE II Cirrus Intensive Field Operation conducted in the state of Kansas in November, 1991. We acknowledge the contributions of the authors of that document for making our task much simpler in producing the following descriptions.

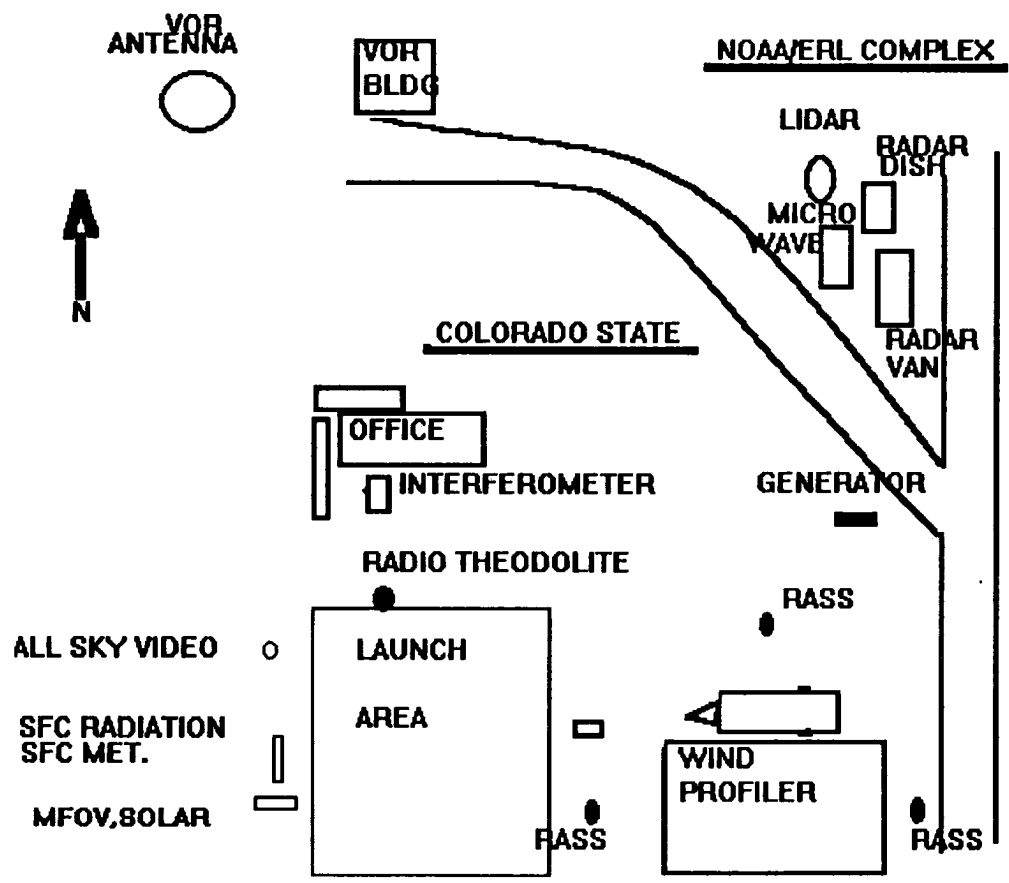


Figure 2: Map of the locations of CSU deployment sites.

Table 1: Surface Meteorology Observations

ASTEX - PORTO SANTO
JUNE 1 - 28, 1992

INSTRUMENTATION	VARIABLES MEASURED	DERIVEABLE PARAMETERS	SAMPLING	AGENCY/INSTITUTION
Campbell 21X System	Temperature Relative Humidity Wind Speed Wind Direction	Same as measured variables	Continuous, 2 min. interval	CSU

Table 2: Infrared Radiation Observations

ASTEX - PORTO SANTO
JUNE 1 - 28, 1992

INSTRUMENTATION	VARIABLES MEASURED	DERIVEABLE PARAMETERS	SAMPLING	AGENCY/ INSTITUTION
Pyrgeometer	3-50 μ m irradiance	Cloud emittance, effective radiating temperature, cloud base temperature	Continuous, 2 min. interval	CSU & WPL
PRT - 6, PRT - 5	10-11 μ m; 8-10 μ m radiance 2 degree FOV, vertical	Cloud base temperature, Cloud emittance, effective radiating temperature	Continuous, 10 sec. interval	CSU, WPL respectively
Infrared interferometer	5-15 μ m; 1 cm ⁻¹ spectral radiance, vertical and angle scan	Temperature(z), cloud spectral emittance, atmospheric spectral emittance, equivalent emitting temperature, trace constituent marker	On demand	CSU

Table 3: Solar Radiation Observations

ASTEX - PORTO SANTO
JUNE 1 - 28, 1992

INSTRUMENTATION	VARIABLES MEASURED	DERIVEABLE PARAMETERS	SAMPLING	AGENCY/ INSTITUTION
Pyranometer	.3-2.8 μ m irradiance .695-2.8 μ m irradiance	Global radiation, Diffuse component w/ Pyrheliometer	Continuous 2 min. interval	CSU & WPL CSU
Pyrheliometer	.3-2.8 μ m direct solar .53-2.8 μ m direct solar .695-2.8 μ m direct solar 1.0-2.8 μ m direct solar All 5 degree FOV (1/2 angle)	Direct component, aerosol extinction coefficient, cloud optical depth	Continuous 2 min. interval	CSU
Sun Photometer	0.50 μ m	Aerosol extinction coefficient	On demand	CSU/ WPL
Multiple Field of View Radiometer	2°,5°,10°,20° and 30° fields of view, Spectral band pass .4 to 1.1 μ m	Cloud optical depth, droplet/crystal size	Continuous 2 min. interval	CSU

Table 4: Cloud Observations

ASTEX - PORTO SANTO
JUNE 1 - 28, 1992

INSTRUMENTATION	VARIABLES MEASURED	DERIVEABLE PARAMETERS	SAMPLING	AGENCY/ INSTITUTION
Scanning 6.8 mm Radar	radar cross section as a function of height, doppler shifted frequency	liquid/ice water content; radial component of velocity; particle fall velocity; cloud base/top height	Continuous	WPL
Scanning 10.7 μm Doppler Lidar	back scatter coefficient as a function of height, doppler shifted frequency	radial component of velocity; cloud base/top height; aerosol backscatter	On demand	WPL
.9 μm Laser Ceilometer	back scatter efficiency as a function of height	Cloud base height	Continuous 1 min repetition	CSU
Video all sky camera	cloud imagery	cloud cover, cloud type	Continuous	CSU

Table 5: Upper Air Observations¹

ASTEX - PORTO SANTO
JUNE 1 - 28, 1992

INSTRUMENTATION	VARIABLES MEASURED	DERIVEABLE PARAMETERS	SAMPLING	AGENCY/ INSTITUTION
Rawinsonde	Temperature (z) Relative Humidity (z) Horizontal wind components (z)	Thickness, precipitable water, stability, dry/moist static energy	one per 3 hours	CSU
404 Mhz Wind Profiler	Backscatter signal strength (z), doppler shifted frequency (z)	Horizontal wind velocity, vertical wind velocity	Continuous 1 wind set/10 min.	CSU
Radio acoustic sounding system [RASS]	velocity of sound(z)	Temperature (z)	one sounding per hour	CSU

¹ The NOAA/WPL radar and lidar also produce air motion information.

Table 6: Summary of CSU ASTEX Data
 May 30 - June 29 1992
 Colorado State University
 Porto Santo Site

Data Set	May		June																													
	30	31	1	2	3	4	5	6	7	8	9	10	11	12	13	14	15	16	17	18	19	20	21	22	23	24	25	26	27	28	29	
Station 1	x	x	x	x	x	x	x	x	x	x	x	x	x	x	x	x	x	x	x	x	x	x	x	x	x	x	x	x	x	x	x	x
Station 3			x	x	x	x	x	x	x	x	x	x	x	x	x	x	x	x	x	x	x	x	x	x	x	x	x	x	x	x	x	x
Wind Profiler /RASS	x	x	x	x	x	x	x	x	x	x	x	x	x	x	x	x	x	x	x	x	x	x	x	x	x	x	x	x	x	x	x	x
Ceilometer	x	x	x	x	x	x	x	x	x	x	x	x	x	x	x	x	x	x	x	x	x	x	x	x	x	x	x	x	x	x	x	x
Sky Camera			x	x	x	x	x	x	x	x	x	x	x	x	x	x	x	x	x	x	x	x	x	x	x	x	x	x	x	x	x	x
Rawinsonde	1	1	7	6	6	6	6	6	5	6	7	7	8	8	8	8	6	8	8	8	10	8	8	8	8	8	8	8	8	8	8	8
Other:																																
Interferometer						6	12					12	6	15	15			6	18	60	15	12	78	78	99	24	42	41	99			
PRT-6			x	x	x	x	x	x	x	x	x	x	x	x	x	x	x	x	x	x	x	x	x	x	x	x	x	x	x	x	x	x

Table 6, Continued

Variables Measured:

Station 1 - (Porto Santo)

Air temperature

Relative humidity

Wind speed

Wind direction

Downwelling solar irradiance

Downwelling near-infrared irradiance

Downwelling infrared irradiance

Direct solar radiance

Direct filtered solar radiance

Station 3 - (Porto Santo)

Sunphotometer

Multiple field of view photometer

2.0 Surface Meteorology

2.1 Campbell Surface Station

The surface radiation and meteorological data collections employed data loggers from Campbell Scientific Inc.

Data were downloaded once each day. The data were initially stored on 740 kbyte floppy disks in a comma-delineated ascii format. This data was archived to Exabyte tape from a 386 PC using the Novaback backup utility, and is also archived under the Firedata account on a Sun Sparcstation I workstation.

2.2 Temperature and Relative Humidity



Figure 3: Surface Instrumentation:

Lower left: Filtered and unfiltered pyrheliometer; Center: Model #207 temperature and relative humidity unit; Upper right: Wind speed and direction sensor.

The Campbell Model 207 unit measures temperature and relative humidity using two sensors combined into one probe. Separate CR10 input/output

instructions are used to read each variable. The probe was mounted on an H frame with a radiation shield.

The probe contains a Phys-Chemical Research PCRCII RH sensor and a Fenwal electronics UUT50J1 thermistor configured for use with CSI's CR10 data logger.

The instruction used to read the temperature sensor provides a 2V AC excitation, makes a single ended measurement, and linearizes the result with a polynomial to output temperatures in °C.

The instruction used to read RH sensor provides a 1.5V AC excitation, makes a single ended measurement and linearizes the result with a fifth order polynomial to provide the % RH parameter. It performs the required temperature compensation before outputting the result.

The following are the linearization errors:

Thermistor		
-40 to 55 °C		≤ 1 °C
-35 to 48 °C		≤ .1 °C
RH sensor		
10 to 100%		≤ 4%
15 to 94%		≤ 1%

The temperature compensation for the relative humidity is given by:

$$RH = RH + .36(25-T)$$

where T - temperature of the air in deg C.

The accuracy of the measurements for the temperature sensor depend on a combination of Fenwal's interchangeability specification, precision of bridge resistors and linearization errors. The overall accuracy is ±.2 °C.

The accuracy of the RH sensor is a combination of the RH chip, precision resistors, and linearization error. The overall accuracy is quoted as better than 5% in the range 12% to 100%.

For additional information on the data gathering system, data storage or data location, see section 2.1.

2.3 Wind Direction and Speed

Wind Speed Measurements:

Range	-	0 to 60 m/s (80 m/s gust survival)
Sensor	-	18 cm 4 blade helicoid propeller
Pitch	-	29.4 cm
Distance constant	-	2.7 m for 63% recovery
Threshold sensitivity	-	.9 m/s
Transducer output	-	100 mV p-p at 60 rpm
	-	20 V p-p at 12000 rpm

Wind Direction Measurements:

Range	-	360° mechanical, 355° electrical
Sensor	-	Balanced vane 38 cm turning radius
Damping ratio	-	.25
Delay distance	-	1.3 m for 50% recovery
Threshold sensitivity	-	1.0 m/s at 10° displacement 1.5 m/s at 5° displacement
Transducer	-	.25% linearity-rated 1 watt at 40° C, 0 watts at 125° C

Wind speed and direction were monitored using a propeller anemometer manufactured by R. M. Young. The main housing, nose cone, propeller, tail, and internal parts are injection-molded, uv-stabilized plastic. The propeller rotation produces an AC sine wave signal with frequency proportional to wind speed. Three complete sine wave cycles are produced for each propeller revolution.

Vane position is transmitted by a 10K ohm precision conductive plastic potentiometer. The output signal is an analog voltage directly proportional to azimuth angle.

The propeller anemometer was mounted on an H frame stand and is calibrated before shipment. It requires no adjustments.

References:

- Campbell Scientific, 1983: Model 207 Temperature and Relative Humidity Probe Instruction Manual. Campbell Scientific, Inc., P.O. Box 551, Logan, Utah 84321.
- Cox, et al., 1992: CSU FIRE II Cirrus Field Experiment: Description of Field Deployment Phase. Colorado State University, Department of Atmospheric Science, Paper No. 506, 55 pgs.
- 21X Micrologger Instrumentation Manual. Revision: 21X.1M. Copyright, 1984. Campbell Scientific, Inc., P.O. Box 551, Logan, Utah 84321.
- CR10 Measurement and Control Module Operations Manual. Revision: 11/88. Copyright 1986, 1988. Campbell Scientific, Inc., P.O. Box 551, Logan, Utah 84321. Scientific, Inc.
- R. M. Young Co., 1988: Wind and Temperature Instruments, Wind Monitor - Model 05103.

3.0 Infrared Radiation

3.1 Pyrgeometer



Figure 4: Surface irradiance sensors:

Left: .695-2.8 micrometer pyranometer; Center: .3-2.8 micrometer pyranometer; Far right: 3-50 micrometer pyrgeometer.

Sensitivity	-	5 $\mu\text{V}/\text{Watt}/\text{m}^2$
Impedence	-	700 ohms
Temperature Dependence	-	$\pm 2\%$ (-20° C to 40° C)
Linearity	-	$\pm 1\%$ (0 to 700 watts/m ²)
Response Time	-	2 seconds
Cosine Response	-	< 5% from normalization (Insignificant for a diffuse source)

An Eppley Precision Infrared Pyrgeometer was used to measure terrestrial irradiance in the 4-50 μm spectral region. It uses a blackened multi junction thermopile to produce a voltage which is related to the incident radiant power. The thermopile is coated with Parsons black lacquer and emits like a black body at a temperature T. A thermistor is used to measure the sink temperature of the thermopile (see figure below).

Spectral bandpass isolation is achieved with a single dome of silicon with a vacuum-deposited interference filter on the inside of the dome.

The orientation of the instrument has no effect on performance, but the accuracy of the instrument is very dependent on calibration which requires special care due to the dome-sink temperature differences.

The following constants were determined for the pyrgeometer monitoring the downwelling irradiance:

$$\text{Station 1: } K_1 = -243.309 \text{ } \mu\text{m}^2/\text{mv} \qquad K_2 = 3.85$$

Using the reduction equations from Albrecht and Cox, 1976, the incident radiance, L , upon the pyrgeometer is given by the following equation.

$$L = K_1 E + \epsilon_o \sigma T_s^4 - K_2 \sigma (T_d^4 - T_s^4)$$

T_s	-	sink temperature
T_d	-	dome temperature
L	-	incident radiation
E	-	voltage
ϵ_o	-	emmittance of thermopile surface
σ	-	Stefan Boltzman Constant

For any additional information concerning data gathering systems, data storage or data location.

Data are archived on 5 1/2 inch floppy disks and on Exabyte tape.

References:

Albrecht, B. A. and S. K. Cox, 1976: Pyrgeometer data reduction and calibration procedures. Department of Atmospheric Science, CSU, Paper No. 251, 1-16.

Cox, et al., 1992: CSU FIRE II Cirrus Field Experiment: Description of Field Deployment Phase. Colorado State University, Department of Atmospheric Science, Paper No. 506, 55 pgs.

_____ : Technical Specifications Brochure, Eppley Laboratory, Inc. Instrumentation for the measurement of the components of solar and terrestrial radiation, 36 pages.

3.2 PRT-6 Infrared Radiometer

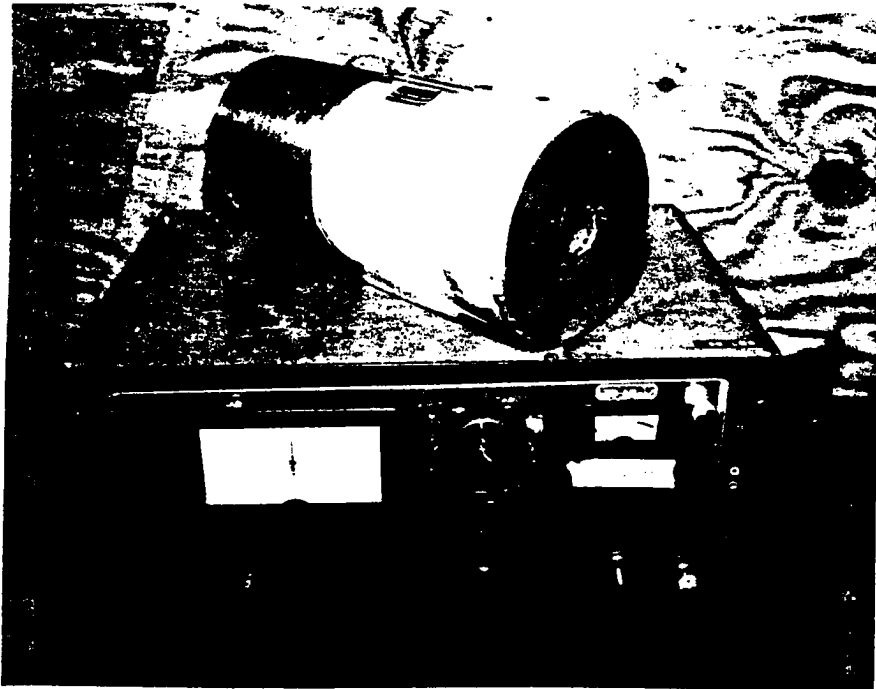


Figure 5: PRT-6 infrared radiometer (11 micrometers).

3.21 The Instrument

The PRT-6 radiometer is a chopped bolometer which can passively sense infrared targets within the spectral range of 2 to 20 microns. The radiometer is configured to accept optics with either a 2 or 20 degree field of view. The output is a voltage signal sampled at a frequency of 1/0.1 sec. The average of the sampled voltage was recorded every 10 seconds, which is nominally linear with respect to the incident radiant power.

In order to operate the instrument continuously in an unattended mode, a section of plastic pipe 5 cm in diameter and 20 cm long was attached to the radiometer head. Forced air was supplied through the side wall of the pipe resulting in an upward flow of air out of the pipe. This flow of air protected the instrument optics from precipitation and thus allowed continuous operation.

3.22 Capabilities and Specifications

For the FIRE II ASTEX deployment the instrument was configured with a field of view of 2 degrees and made use of an interference filter whose transmission curve is displayed in Figure 5. This filter effectively limited the spectral bandpass to 885 to 945 inverse centimeters. Most of the measurements were made with the instrument pointing vertically upward, although for brief intervals zenith angles of 15, 30, 45, 60, and 75 degrees were also utilized.

During the experiment an electrical attenuation component was sometimes added to the instrument to maintain the readings to within -10 and 10 volts, the range of linearity. The resulting attenuation factor was 1.98 and its use or lack thereof is listed in the data file listing.

3.23 The Data

The data retrieval system used was a Campbell Scientific, Inc. datalogger unit which stored the data in the format displayed in Table 7, where the parameters of each line reveal the date, the Z time in hours and minutes, seconds, and the output voltage reading, respectively. Data were recorded every 10 seconds and archived on floppy diskettes and later on Exabyte tape.

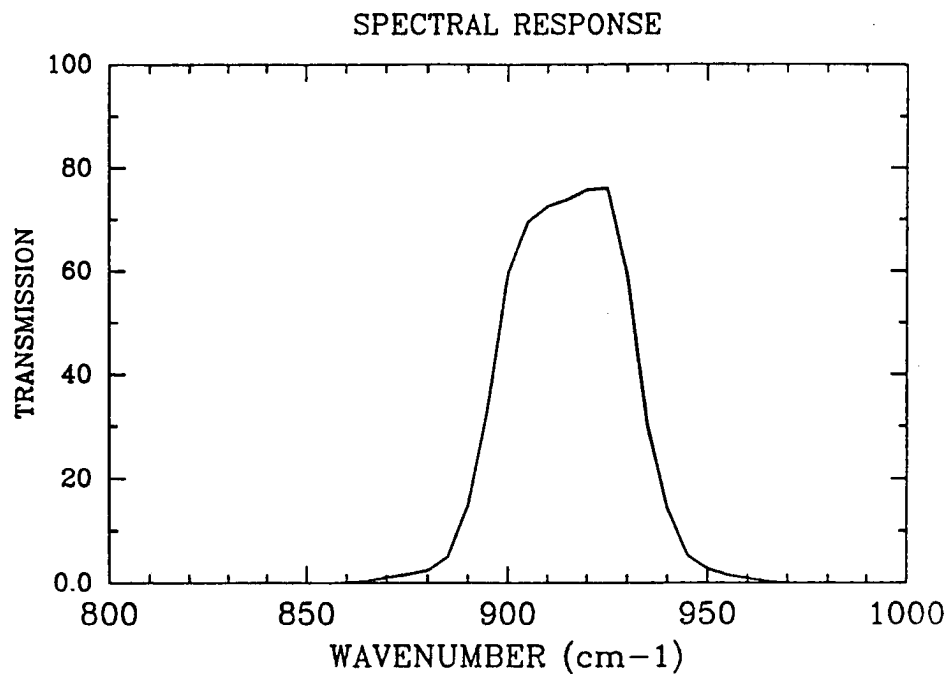


Figure 6: PRT-6 spectral response curve

Table 7: Format of the PRT-6 data recorded in the datalogger. Although the format of the calibrated data is in a different form, both datasets can be accessed by the FORTRAN command "READ(*,*)".

Day No.	GMT Hrs., Mins.	Sec.	Voltage mv
204	2210	52	-1379
204	2210	57	-1383
204	2211	2	-1386
204	2211	7	-1389
204	2211	12	-1391
204	2211	17	-1392
204	2211	22	-1395
204	2211	27	-1397
204	2211	32	-1401
204	2211	37	-1404

3.24 Calibration of the PRT6

In order to calibrate the PRT6 it is necessary to derive a constant k such that, $\bar{N} = k V_{PRT6}$, where N is the downwelling radiance and the overbar indicates an average over the spectral bandpass and V_{PRT6} is the voltage output of the radiometer. Actually one can think of the voltage as responding to an input spectral radiance N_ν according to;

$$V_{PRT6} = \frac{1}{k} \int_{\nu_1}^{\nu_2} N_\nu f(\nu) d\nu, \quad (1)$$

where $f(\nu)$ is the filter response function used, which in this case, may be defined by the spectral limits from 865-965 cm^{-1} . The PRT6 will provide only an average radiance within the spectral interval so we define k by;

$$V_{PRT6} = \frac{1}{k} \bar{N} \int_{\nu_1}^{\nu_2} f(\nu) d\nu, \quad (2)$$

which requires that;

$$\bar{N} = \frac{\int_{\nu_1}^{\nu_2} N_\nu f(\nu) d\nu}{\int_{\nu_1}^{\nu_2} f(\nu) d\nu}. \quad (3)$$

In the initial calibration procedure the values of N were obtained without taking the filter response function into account. The values of N_ν were obtained from the calibrated spectra of a Bomem MB-100 interferometer for clear sky, cirrus overcast and stratocumulus overcast cases. The values V_{prt6} were averaged over the time period (1.5 minutes) required to collect the corresponding atmospheric interferogram. That original calibration was carried out essentially as if $f(\nu) = 1.0$, and the integration was confined within the bandwidth of the half-maximum points (897-935 cm^{-1}) of the PRT6 filter. A more complete analysis shows that the average radiance calculated by the above equation using the bandwidth within the half maximum points and including the filter response is nominally 2% lower than the original method. The results are worse (5%) for a 200 K black body curve, but were found to be only 2% for a cirrus layer between 9.5 and 11.0 km on 26 Nov 1991.

However it was also found that using the full spectral bandpass and taking the filter response into account as in the last two equations results in radiances which are within 0.2%, 2.2% and virtually 0% for the clear sky, 200 K black body and cirrus cases respectively. This occurs since a radiance integrated over the full spectral bandpass is only about 2% greater than one integrated over the bandpass within the half-maximum points.

The PRT-6 absolute calibration in radiance units was conducted by integrating the observed interferometer spectra over the PRT-6 spectral bandpass for a number of coincident observing periods. The linear relationship resulting from this calibration is shown in Figure 7.

Appendix 2 gives a statement by statement summary of commands used in "Spectra Calc", a commercially available software package, to integrate the interferometer data for this calibration. The resulting empirical equations relating voltage output to radiance and to equivalent black body temperature are given in equations 4 and 5 below, respectively.

$$N[w\text{ cm}^{-2}\text{ ster}^{-1}]_{897-935\text{ cm}^{-1}} = 725.248 + 0.90941 * MV, \quad (4)$$

where MV is the PRT6 output voltage expressed in millivolts.

A second order polynomial expression to convert radiance to equivalent black body temperature (Brightness temperature) for the PRT 6 spectral bandpass is:

$$T_{brt} [deg\ K] = 186.0245 + 0.38633 * N - 0.0003 * N^2. \quad (5)$$

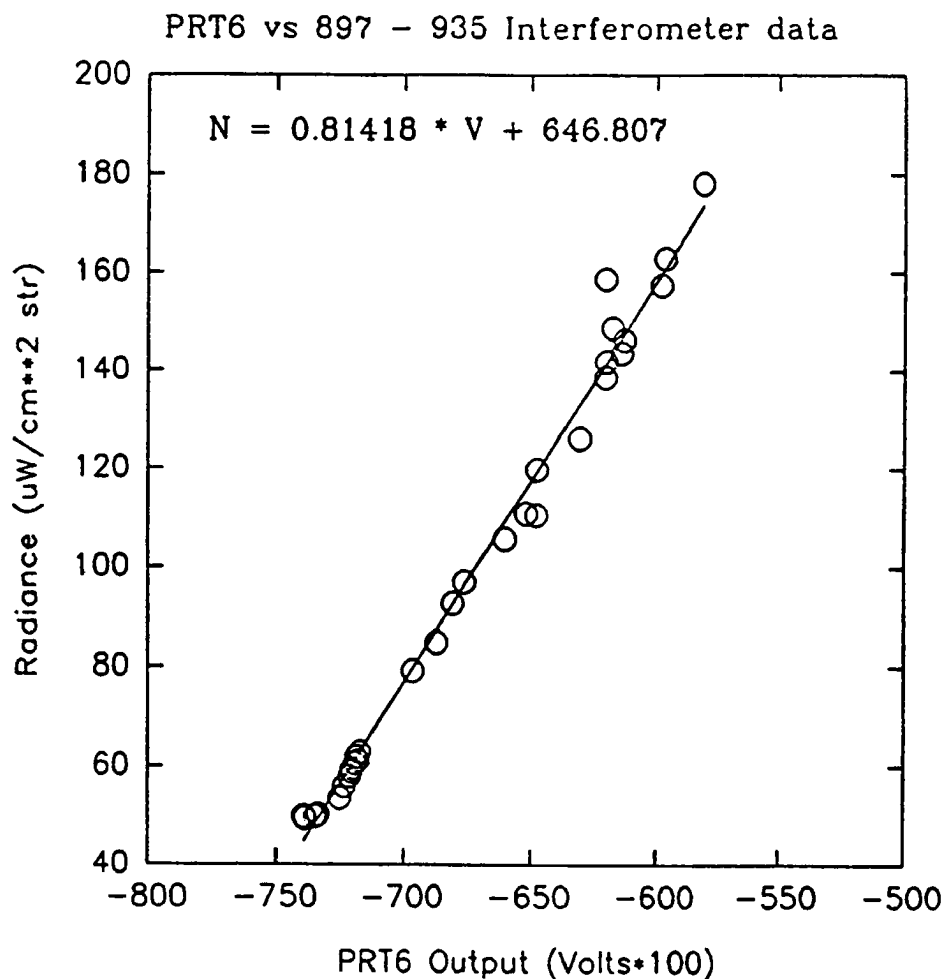


Figure 7: Calibration curve.

3.3 Infrared Interferometer

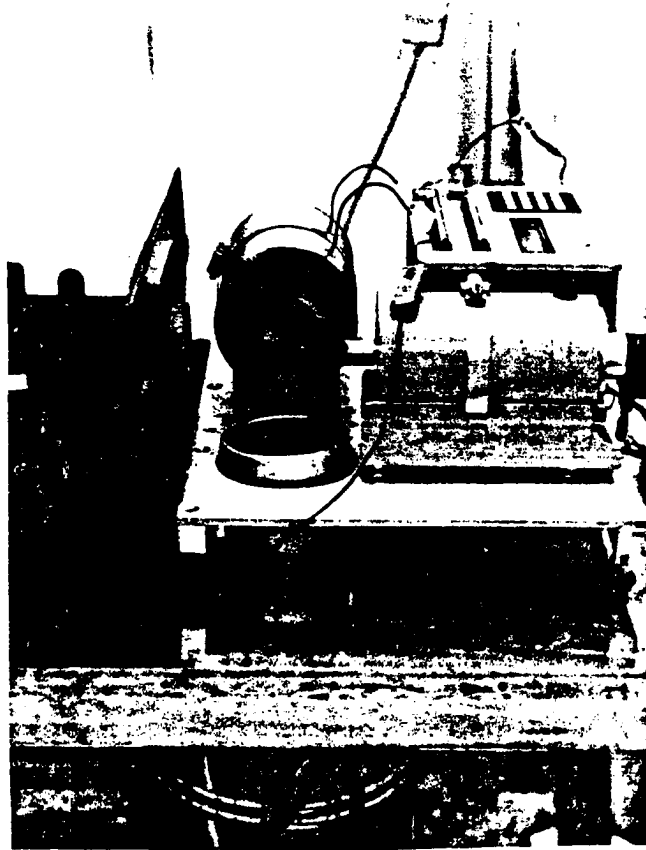


Figure 8: Infrared interferometer and calibration system.

The instrument used in this experiment was a dual port emission interferometer manufactured by Bomem, Inc. It has an adjustable resolution ranging from 1 cm^{-1} to 128 cm^{-1} . ASTEX data were taken with the interferometer at the 1 cm^{-1} resolution setting. The detector is cooled cryogenically using high pressure N_2 gas. The useful range of the detector is from 500 to 2000 cm^{-1} .

One port views a reference blackbody and is protected by a desiccant container. This reference blackbody is attached directly outside the second interferometer port and it consists of a copper element maintained at a temperature slightly above ambient and grooved and coated to improve the emissivity. The reference blackbody temperature is monitored by a small thermocouple which is located within 5 ten thousandths of an inch beneath the surface of the coated side.

Facing the target port of the interferometer is a rotatable gold-plated mirror mounted at a 45 degree angle with respect to the axis of the entering optical path. The position of this mirror is maintained by a computer controlled DC servo motor and control circuit, enabling the interferometer to scan the atmosphere at various zenith angles.

3.31 Schematic of the Optical Path

The interferometer views the atmospheric emission through a KBr window following reflection by rotatable gold-plated mirror. The beam then enters into a Michelson interferometer. The radiation from the reference blackbody in the reference port also enters the Michelson interferometer. This beam however is 180 degrees out of phase with the atmospheric emission beam which results in the generation of a difference interferogram at the detector module.

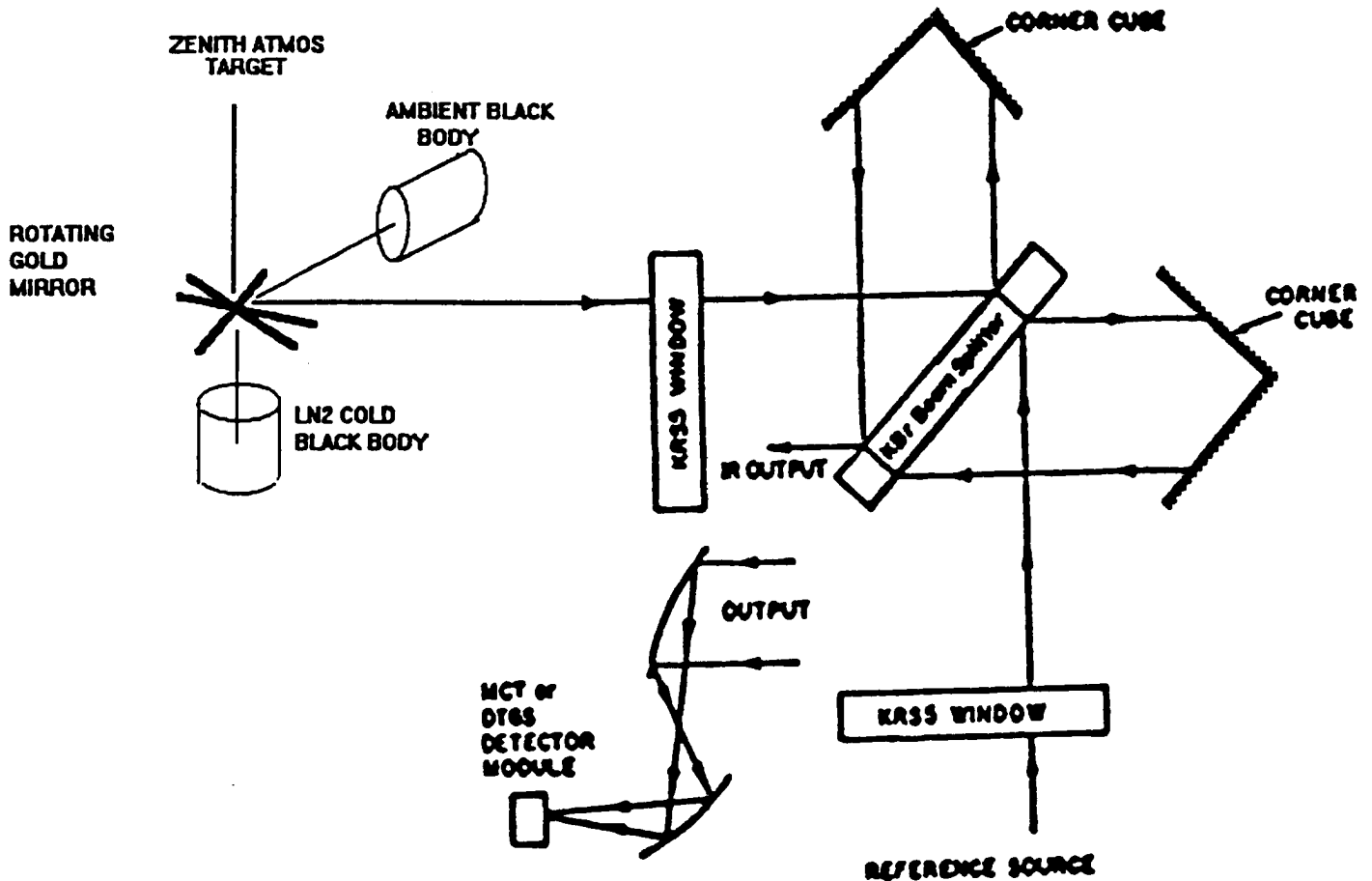


Figure 9: Schematic of the optical path of the dual port interferometer system.

3.32 Calibration and Measurement

3.321 Blackbody sources

Two blackbody sources are used to calibrate the interferometer. A cold blackbody source is a dewar of liquid nitrogen which is known to be at 77 K. The other blackbody used in the calibration is a warm blackbody source that is made out of copper. Its cavity is coated to insure a high surface emissivity. The copper blackbody is at the ambient air temperature; two small thermocouples located near the inner walls of the copper blackbody monitor the temperature. For the calibration of the instrument, it is necessary to record the emission at each wavenumber from each of the two blackbody sources. It is practical to use the liquid nitrogen since it is preferable that the two sources bracket the emission temperature of the atmospheric beam.

The mirror is controlled by PC software such that the interferometer sequentially views the liquid nitrogen followed by the copper blackbody and then the atmosphere.

3.322 Data Storage

One data collection cycle includes viewing the two blackbody sources and the atmosphere. In the ASTEX experiment each cycle consisted of 20 interferometric scans for each mirror position which are co-added to reduce the noise of the measurement. This yields three interferograms. The temperatures of the reference blackbody, the warm and cold blackbody sources, and the ambient air are measured every 0.2 seconds. Every 100 temperature measurements are averaged and are then recorded at 20 second intervals on a CR21X Campbell Scientific, Inc. datalogger. The temperature data are then downloaded to the PC which operates the interferometer. Each cycle takes slightly less than two minutes to complete, resulting in five temperature readings per object.

3.323 Brief Outline of Calibration Procedure

The data which are taken during each set of 20 scans by the interferometer is an interferogram which may be represented by Eq. (6):

$$F(x) = \frac{1}{2} \int_{-\infty}^{\infty} C_{\nu} \exp[i\phi(\nu)] \exp[i2\pi\nu x] d\nu \quad (6)$$

This interferogram can be processed by Fourier transform to a difference spectrum. The uncalibrated spectrum in terms of radiances may be written as:

$$C_{\nu} = |\tilde{F}| = r_{\nu} (L_{\nu} + L_{\nu}^{\circ}) \quad (7)$$

where: x is the optical path delay
 ν is the wavenumber in cm^{-1}
 $\phi(\nu)$ is the phase response of the instrument
 r_{ν} is the responsivity of the instrument
 L_{ν} is the spectral emission
 L_{ν}° is the offset emission of the instrument
 \tilde{F} is the complex Fourier transform

Equation (7) shows the linear relationship between the uncalibrated spectrum and the spectral emission. The response of the detector and the offset are two unknowns to be derived from the calibration. These unknowns can be found from observing the cold and hot blackbody sources.

The responsivity of the interferometer may be written as:

$$r_{\nu} = (C_{h\nu} - C_{c\nu}) / [B_{\nu}(T_h) - B_{\nu}(T_c)] \quad (8)$$

and the offset required may be written as:

$$L_{\nu}^{\circ} = \frac{C_{h\nu} - C_{r\nu}}{r_{\nu}} - B_{\nu}(T_h) \quad (9)$$

where $B_{\nu}(T)$ represents the Planck function, the subscripts h and c refer to the hot and cold blackbodies respectively, and r refers to the reference blackbody. Now, with the known detector response and

offset required, the atmospheric emission can be found and may be written as:

$$L_v = \frac{C_v}{r_v} - L_v^o \quad (10)$$

The interferograms are actually difference interferograms between the desired target and the reference blackbody, and since the reference blackbody temperature can be maintained to 0.1 C, the uncalibrated reference spectra (C_{rv}) subtracts out of equations (8) and (10). The calibration of the interferometer within the range of interest is within 2%.

Examples of spectra are shown in Figures 10a, b.

Interferogram and calibrated spectra data are archived at Colorado State University in a compressed format on exabyte tape.

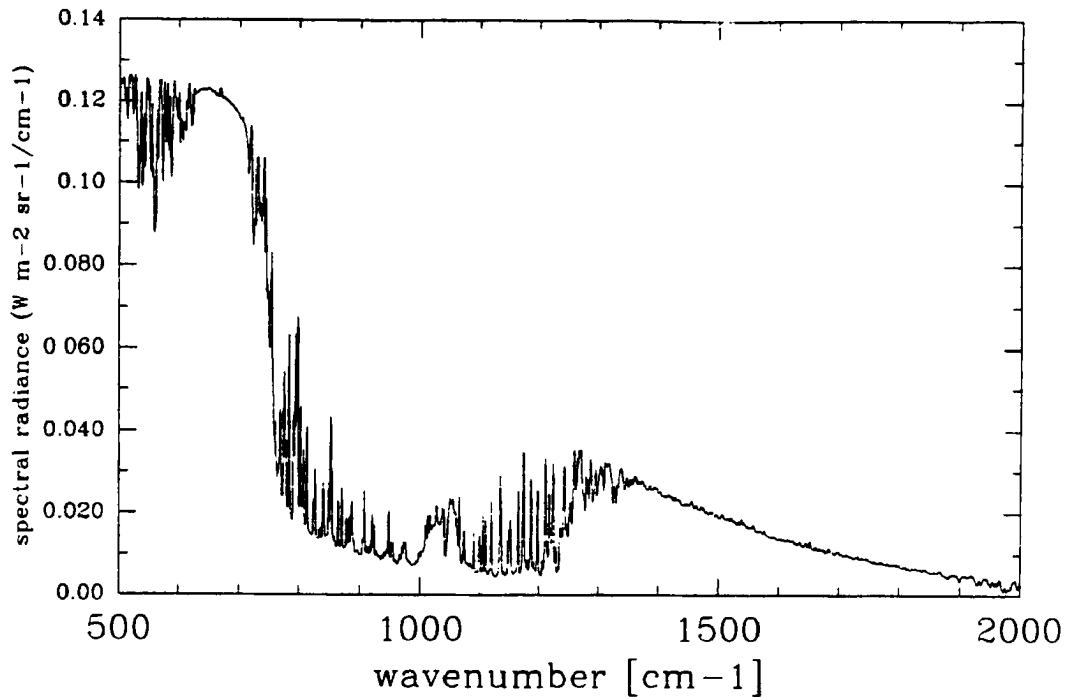


Figure 10a: Example of a clear sky infrared spectrum observed.

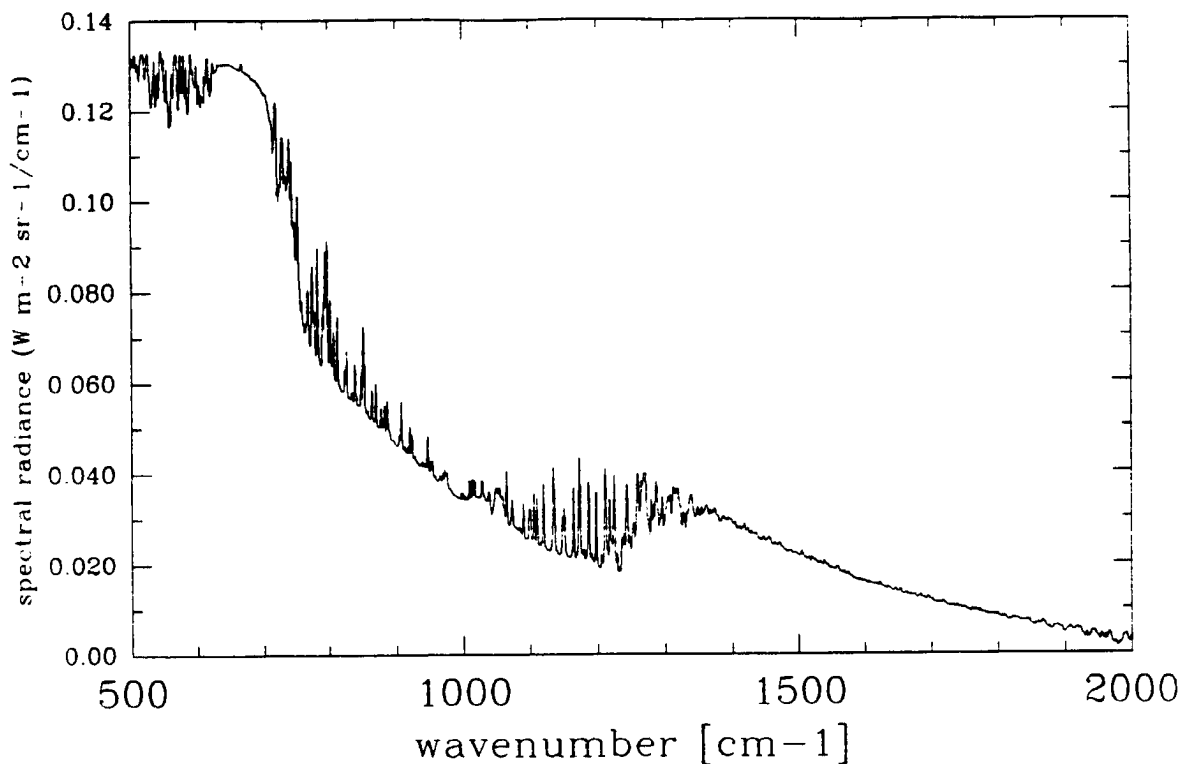


Figure 10b: Example of an infrared spectrum observed in the presence of cirrus clouds.

References:

Cox, et al., 1992: CSU FIRE II Cirrus Field Experiment: Description of Field Deployment Phase. Colorado State University, Department of Atmospheric Science, Paper No. 506, 55 pgs.

Revercomb, H. E., et al., 1988: Radiometric calibration of IR Fourier transform spectrometers: solution to a problem with the high-resolution interferometer sounder. *Applied Optics*, 15, 3210-3218.

4.0 Solar Radiation
(See Figure 4, section 3.1)

4.1 Pyranometer
(See Figure 4, Section 3.1)

Sensitivity	~	9 $\mu\text{V}/\text{watt}/\text{m}^2$
Impedence	~	650 ohms
Temperature Dependence	~	$\pm 1\%$ over ambient temperature (20°C to 40°C)
Linearity	~	$\pm .5\%$ (0 to 2800 watt/m^2)
Response Time	~	1 second
Cosine Response	~	$\pm 1\%$ from normalization (0 to 70° zenith)
	\pm	3% from normalization (70° to 80° zenith)

An Eppley Precision Spectra Pyranometer (PSP) was used to measure shortwave irradiance.

The PSP uses a multi junction thermopile blackened with Parsons black lacquer which is temperature compensated to give a response independent of ambient temperature.

The pyranometers have two concentric hemispheres of precision ground and polished Schott optical glass. The inner hemisphere on both pyranometers was WG7 clear glass transparent from .28 to 2.8 μm . On one pyranometer the outer dome was also WG7; the other used RG695 dark red glass transparent from .695 to 2.8 μm .

The accuracy of the PSP is typically 1%. It should be noted, calibrations could have a diurnal and annual cycle arising from geometric arguments.

The instruments used in these experiments were compared with secondary standards to establish calibration coefficients relating the voltage output of the instruments to the irradiance. The following calibration coefficients were obtained and compared with pyranometer calibrations at NOAA CMDL:

$H(w/m^2) = aV + b$	<u>Slope</u> $a(W\ m^{-2}\ mv^{-1})$	<u>Y intercept</u> $b(w\ m^{-2})$
Station 1 - WG7	117.246	0
Station 1 - RG695	102.1832	0

where V is the measured voltage output expressed in mv.

For additional information concerning the data gathering system and data storage see section 2.1.

Reference:

_____ : Technical Specifications Brochure, Eppley Laboratory, Inc. Instrumentation for the measurement of the components of solar and terrestrial radiation, 36 pages.

4.2 Pyrheliometer

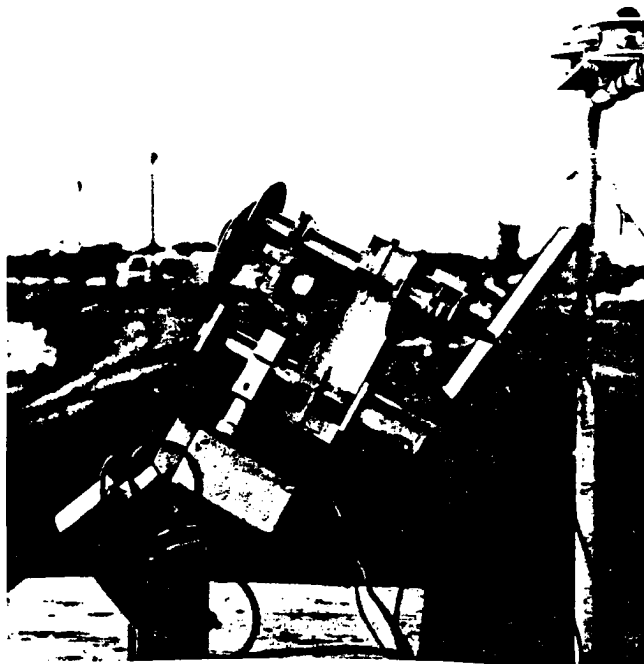


Figure 11: Filtered and unfiltered pyrheliometer (see also figure 3, section 2.2).

Specifications:

Temperature Range	-	-20 to 40° C (1% accuracy is achieved by a special temperature compensation circuit.
Response Time	-	98% of maximum output is achieved in 20 seconds
Output	-	3.0-3.5 $\mu\text{v}/\text{cal}/\text{cm}^2/\text{min}$.
Internal Resistance	-	400 ohms at 25° C
Emf	-	8.82×10^{-6} volts/watt/m ² (after comparisons with Eppley group reference standards under radiation intensities from 700 to 888 watt/m ²)
Linearity	-	within .5% of the above intensity
Field of view	-	5° 43' (half angle)

The Eppley pyrhelimeter measures the direct component of solar radiation incident upon a surface perpendicular to the solar beam.

The detector consists of a thin 9 mm silver disc coated with Parsons optical black lacquer. Fifteen junctions of fine bismuth silver thermocouples are in thermal contact with, but electrically insulated from the lower surface of the disc. The cold junctions are in thermal contact with the copper tube of the instrument. A rotatable frame for three filters is provided. The receiver rotates allowing timed readings from each filter. The following filters were used:

		<u>Spectral Bandpass</u>
Channel 1	Schott filter	.53 - 2.8 μm .
Channel 2	Schott filter	.695 - 2.8 μm .
Channel 3	Schott filter	1.0 - 2.8 μm .
Channel 4	WG 7 Quartz dome	.3 - 2.8 μm .

Two pyrhelimeters tracked the sun using a LI 2020 solar tracker. One pyrhelimeter came direct from the factory with a factory calibration constant of 8.82×10^{-6} volts/watt/m². This pyrhelimeter sequentially sampled channels 1-4 with a 15 second dwell time on each channel. The second pyrhelimeter made observations in the channel 4 spectral bandpass only.

Data are archived at NCDS.

References:

Cox, et al., 1992: CSU FIRE II Cirrus Field Experiment: Description of Field Deployment Phase. Colorado State University, Department of Atmospheric Science, Paper No. 506, 55 pgs.

_____ : Technical Specifications Brochure, Eppley Laboratory, Inc. Instrumentation for the measurement of the components of solar and terrestrial radiation, 36 pages.

4.3 Multi Field of View Radiometer (MFOV)

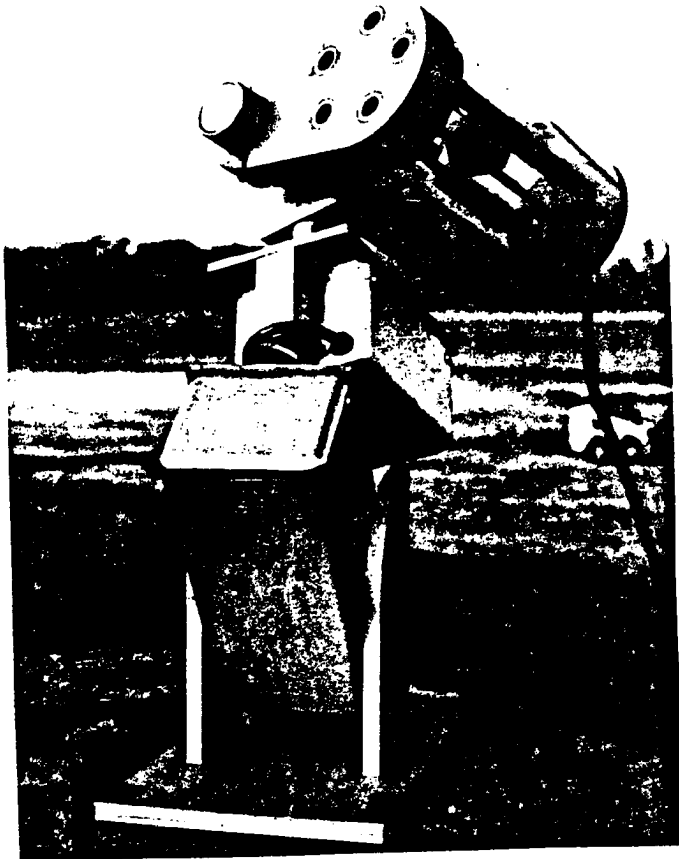


Figure 12: MFOV Radiometer

From the MFOV measurements, one may infer the optical depth of clouds and the equivalent Mie size characteristics of the scattering medium. This is achieved by measuring the solar irradiance in five different fields of view centered on the solar disk.

The MFOV utilizes five silicon photodiodes (PV100A series) aligned along a common optical axis each with a different full angle field of view; a spectral bandpass of .35 to 1.15 μm is common to all.

<u>Field of View</u> (degrees)	<u>Length (mm)</u>	<u>Aperture Diameter (mm)</u>
1.9°	146	2.5
2.5°	125	2.5
4.3°	70	2.5
6.5°	45	2.5
11.5°	25	2.5

The interior of the collimator is coated with a flat black lacquer to reduce scattering. The following are the characteristics of the PV100A photodiodes:

Active area	-	5.1 mm ²
Window thickness	-	1.3 mm
Window diameter	-	6.1 mm
Diode length (minus leads)	-	4.2 mm
Diode length (plus leads)	-	< 24.2 mm

The MFOV tracks the sun with a LICOR microprocessor based solar tracker.

The accuracy of the measurements are dependent on instrument calibration. Calibrations were performed at CSU on October 23, 1991 for clear sky cases. Data during the experiments are used to confirm this calibration data.

Data are achieved at CSU on exabyte tape and on a Sun Sparcstation.

Raschke, R. A. and S. K. Cox, 1982: The determination of cloud optical depth from multiple field of view pyrhelimetric measurements. Department of Atmospheric Science, CSU, Paper No. 361, 1-14.

Anikin, P. P., 1991: Determination of the spectral optical thickness and effective particle size of cirrus clouds. *Izvestiya, Atmospheric and Oceanic Physics*, 27, 668-672.

4.4 Sun Photometer



Figure 13: Tracking Sun Photometer

A MAINZ sunphotometer was deployed at the Porto Santo site in order to infer the optical thickness of clouds in the mid-visible portion of the solar spectrum. The photometer is not a completely weather proof instrument and was deployed only during times of interest (see table 2) and only when precipitation posed no threat to instrument integrity.

4.41 Instrument Description

The MAINZ sunphotometer, model MZ II, is a precision electro-optical device which was originally designed to estimate aerosol optical depth. It was designed to be hand held or tripod mounted, and its output signal can be read from an LCD display on the top panel of the instrument. Several features of the instrument pertain to a "stand alone" type of measurement. In its deployment at Porto Santo the output of the instrument was obtained from a 0.0 - 2.0 volt output jack on the instrument, and several of the features (such as a selectable signal amplification, elevation angle measurements and peak signal holding feature) were not pertinent to its operation and will not be discussed here.

The detector employed in the sunphotometer is an EG&G UV 100 BQ, which is a UV enhanced photodiode linear to within 1% for a range of incident irradiances spanning 7 decades. The dark current of the photodiode is 3 nA.

A diopter with a plano convex lens and a surface mirror images the sun on an opaque screen in order to assure proper alignment of the instrument.

A filter wheel allows the selection of 5 interference filters, although only the 0.500 μm filter was used for this deployment. Table 8 summarizes the instrument capabilities.

Table 8: Technical specifications of the MAINZ MZ II - 85 sunphotometer

Model	MAINZ MZ II - 85
Number of channels	5
Peak wavelength in μm	0.38, 0.412, 0.50, 0.675, 0.862
Wavelength accuracy	$\pm 0.001 \mu\text{m}$
Bandwidth	0.002 - 0.005 μm
Transmission	15 - 50 %
Full field of view	2.2°
Slope angle	0.8°
Filter diameter	10 mm
Effective filter diameter	6 mm
Type of detector	EG&G, UV 100 BQ
Relative signal accuracy	0.5 %

4.42 Instrument Deployment

The sunphotometer was deployed on a LICOR model 2020 solar tracker. The solar tracker was mounted approximately 1 meter above the ground and 2 m to the south of the H-Frame station.

As mentioned above, the sunphotometer is not designed for deployment in all types of weather and particularly not during precipitation events. When conditions warranted the instrument was enclosed in a plastic bag containing a large supply of desiccant. The instrument was also covered in this manner during the night to protect it from moisture. Care was taken to keep the instrument aligned and viewing the solar disk; however, because of the photometer's small field of view and imperfect alignment of the solar tracker the user of the data should be aware of possible inaccuracies introduced by slight misalignment. Table 9 lists the periods of data collection.

4.43 Data Collection and Archiving

The data were collected by accessing a 0 - 2 Volt output jack on the side of the photometer. The data were recorded once every 2 minutes, except as noted in Table 9. Data were recorded using a Campbell Scientific, Inc., CR21X data logger. The data were downloaded to a DOS disk and converted to ASCII format. The data are archived in this original format and also in ASCII format on a UNIX workstation. Table 9 details the times of data collection determined from an initial inspection of the archived data. All times are UTC.

Table 9: Dates and times (UTC) of data collected by the Mainz Sun photometer.

Date	Start Time	End Time
07 June 92	06:24	08:30
08 June 92	08:12	17:56
09 June 92	08:02	17:07
10 June 92	07:53	15:50
12 June 92	11:45	16:10
13 June 92	08:15	19:01
14 June 92	11:19	13:53
15 June 92	07:53	17:09
17 June 92	12:46	17:13
18 June 92	08:36	17:52
19 June 92	09:38	17:36
20 June 92	13:59	18:21
22 June 92	12:35	13:40
24 June 92	07:04	07:24
24 June 92	07:56	09:17
24 June 92	15:15	19:59
25 June 92	07:53	19:58
26 June 92	09:27	19:17
27 June 92	09:35	15:20

4.44 Calibration

The data from the sunphotometer are in units of volts. No calibration exists at the current time for converting the signal to irradiance or to optical depth. Some information is contained in the data for clear sky conditions; however, further processing of these data is required to obtain calibration constants. A laboratory calibration will be performed on the sunphotometer using an irradiance standard lamp during spring of 1992.

5.0 Upper Air

5.1 Radiosonde system

Soundings were taken with the Intellisonde Rawin System (Model IS-4A1-MET) manufactured by Atmospheric Instrumentation Research (AIR), Inc., Boulder, Colorado. The AIR system hardware consists of an automatically tracking radiotheodolite (Fig. 14), a PC-AT compatible computer with an AIR Metdecoder board in one of its expansion slots, and a supply of sondes (Intellisonde model IS-4A-1680) and 200 gram balloons. The system provides soundings of pressure, temperature, relative humidity, and the azimuth and elevation angles of the radiotheodolite. The AIR system software also computes real-time derived quantities (e.g., dew-point temperature, geopotential height, winds) but we have chosen to recompute these derived quantities in the post-analysis phase.

The sonde, shown in Fig. 15, is 10cm on the sides, 15cm high and have a mass of 240 grams. The upper third of the sonde consists of a shielded compartment for the humidity sensor. As the sonde rises, air enters the top of the sonde into the hygristor compartment, flows past the hygristor, and then exits through the side of the sonde. The 200 gram balloons were inflated with helium (or, early in the experiment, with hydrogen) to provide approximately $4\text{-}5 \text{ ms}^{-1}$ rise rate, which yields adequate flow past the hygristor. The bottom of the sonde is a ground plane with a downward extending quarter wave antenna for telemetry to the surface. The oscillator frequency on the sonde is 1680 MHz. Power is provided by two 9 volt alkaline batteries. The system has an auto-launch feature which automatically begins data collection when a 0.8 mb change of pressure is detected.

Pressure is measured with an aneroid sensor whose capacitance varies with pressure. The transfer function which translates capacitance to pressure is a fifth-order polynomial whose coefficients are different for each sonde. These calibration coefficients are stored in the sonde and transmitted to the radiotheodolite in the preflight phase, while the sonde is on its prelaunch support stand.



Figure 14: John Kleist (left) and William Cotton prepare for launch under windy, stratocumulus conditions on Porto Santo. Between them is the automatically tracking radiotheodolite, which measures azimuth and elevation angles of the balloon.



Figure 15: AIR Intellisonde, which is 10cm on the sides, 15cm high, and has a mass of 240g. The rod thermistor is on the right. The hygistor is in the radiation shielded compartment at the top of the sonde. As the sonde rises, air enters the inlet at the top, flows horizontally across the hygistor, and the exits downward at the left of the sonde. The sonde transmits at 1680 MHz via a quarter wave antenna which extends from the bottom (not visible).

Temperature and relative humidity are measured with resistive sensors, both manufactured by VIZ. The temperature sensor is a rod thermistor whose lock-in value is printed on the radiosonde body and is entered into the computer in the prelaunch phase. The relative humidity is measured with a VIZ Accu-Lok humidity sensor (a carbon strip hygristor). These sensors are individually calibrated at 25° C and 33% relative humidity. The relative humidity sensor is removed from its sealed foil package and its lock-in value is also entered into the computer before launch.

During ASTEX the radiosonde system was set up at an elevation of 97 m on the north side of Porto Santo Island, which provided good exposure to the prevailing northerly flow. During the period from 1 June to 28 June 1992, 203 soundings were obtained. Observation times, maximum altitudes and observer comments for these soundings are summarized in Appendix 1.

5.11 Analysis of the thermodynamic data

5.111 Time lag effects

Whenever radiosondes ascend through inversions there arise questions about errors due to sensor time lag. Before proceeding to the analysis of the thermodynamic data, let us briefly discuss these effects.

Let T denote the sensor temperature and T_e the environmental temperature. According to the Newtonian cooling law, T and T_e are related by the first order differential equation

$$\frac{dT}{dt} = -\frac{1}{\tau}(T - T_e) \quad (11)$$

where τ is the sensor response time. Let us assume that the environmental temperature changes linearly in time as the balloon ascends so that $dT_e/dt = \lambda$. The above equation can then be written

$$\frac{d(T - T_e)}{dt} + \frac{1}{\tau}(T - T_e) = \lambda \quad (12)$$

which has the solution

$$T - T_e = [(T - T_e)_0 + \lambda\tau] \exp(-t/\tau) - \lambda\tau \quad (13)$$

If we wait long enough for the initial condition $(T - T_e)_0$ to be forgotten, the sensor temperature T and the environmental temperature T_e will differ by $-\lambda\tau$. If the sensor rises at 5 ms^{-1} in an atmosphere with a dry adiabatic lapse rate, then $\lambda =$

-0.05 K s^{-1} . Since the temperature sensor in the AIR sonde has a 3 to 5 s lag constant, $-\lambda\tau \approx 0.2 \text{ K}$, i.e. the sensor reads approximately 0.2 K too warm. On the other hand, if the sensor rises at 5 ms^{-1} through a 100 m thick temperature inversion of 5 K, then $\lambda = 0.25 \text{ K s}^{-1}$ and $\lambda\tau \approx 1.0 \text{ K}$, which means the sensor reads approximately 1.0 K too cold.

The lag of the humidity sensor depends on temperature. At 25° C , the lag constant is between 1 and 2 seconds, at 0° C it is between 3 and 5 seconds, and below -20° C it is between 5 and 10 seconds. If equations similar to those for temperature lags are applied to the humidity sensor, the slow rate of increase of relative humidity in the boundary layer, coupled with a 2 s lag of the hygistor element, causes the sensor to read too dry by only a few tenths of a per cent. However, a 60% decrease in humidity in a 100 m layer above cloud top leads to a sensor reading about 6% too high.

Although these lag effects are not entirely negligible in strong inversions, we have not corrected for them in any way.

5.112 Derived quantities

The raw radiosonde data consists of pressure, temperature, relative humidity, and azimuth and elevation angles as a function of time. The AIR software creates files of these raw data along with several derived quantities. An example is shown in Table 10. Each row consists of time (UTC), pressure, temperature, dew point temperature, relative humidity, geopotential height, azimuth, elevation, wind speed, wind direction, and elapsed time from launch. Several points are worth noting.

First of all, although 2.2 s time intervals are common, the data are not equally spaced in time. To obtain data equally spaced in time or equally spaced in height (determined hydrostatically), interpolation is necessary.

Secondly, although the average rate of pressure change is about -0.5 mb/s (i.e. about 5 m/s rise rate), there are irregularities in plots of pressure versus time. In fact, pressure can sometimes be nonmonotonic with time. Since downdrafts in stratocumulus are unlikely to be strong enough to force the balloon downward, the slight nonmonotonic nature of the pressure profile is probably a deficiency in the aneroid sensor.

Table 10: Sample of Level I data for 2 June 0848 UTC

TIME	PMB	TEMP	TDEW	RH%	GEOPM	AZDEG	ELDEG	SPEED	DIR	E.TIME
07:58:42.35	1008.10	17.10	12.42	74.00	97	134.70	8.05	2.6	10	0.00
07:58:43.42	1007.96	16.88	12.55	75.72	98	148.45	9.38	2.6	10	1.07
07:58:46.52	1006.22	16.70	12.43	75.98	113	152.77	17.02	6.1	353	6.31
07:58:48.66	1005.23	16.63	12.41	76.21	121	154.68	19.08	6.4	352	8.45
07:58:50.81	1004.10	16.55	12.35	76.29	131	156.68	22.10	6.8	352	10.60
07:58:52.95	1002.81	16.45	12.28	76.41	142	157.32	24.55	7.2	351	12.74
07:58:55.15	1001.45	16.36	12.29	76.93	153	157.60	26.98	7.8	351	14.94
07:58:57.29	1000.12	16.27	12.27	77.26	165	161.25	29.30	7.6	351	17.08
07:58:59.43	999.05	16.17	12.25	77.68	174	161.93	29.92	7.4	352	19.22
07:59:01.57	998.18	16.03	11.99	77.03	181	162.38	31.52	7.2	353	21.36
07:59:03.71	997.26	15.92	11.88	77.01	189	164.95	31.52	7.0	353	23.50
07:59:05.91	996.12	15.83	11.82	77.11	199	166.50	30.65	6.8	357	25.70
07:59:08.05	994.91	15.63	11.75	77.75	209	168.15	31.67	6.7	358	27.84
07:59:10.20	993.82	15.53	11.76	78.33	219	167.48	31.10	6.8	358	29.99
07:59:12.39	992.90	15.46	11.79	78.84	226	167.73	30.95	6.8	359	32.18
07:59:14.53	992.19	15.38	11.80	79.31	233	169.43	30.45	6.4	360	34.32
07:59:16.73	991.08	15.29	11.87	80.11	242	168.40	29.92	6.2	2	36.52
07:59:18.87	990.28	15.22	11.92	80.79	249	168.55	29.92	6.2	2	38.66

Table 10, Continued

Sample of Level II data for 2 June 0848 UTC

	z(m)	P(mb)	T(c)	Td(c)	SPEED (m/s)	DIRECTION (degrees)
1	97	1008.10	17.10	12.42	2.60	10.00
2	100	1007.89	16.87	12.57	11.04	328.63
3	110	1006.70	16.75	12.48	8.79	309.83
4	120	1005.51	16.65	12.43	6.82	327.35
5	130	1004.33	16.57	12.38	5.83	326.02
6	140	1003.14	16.48	12.31	6.19	329.96
7	150	1001.96	16.39	12.30	5.36	340.61
8	160	1000.78	16.31	12.30	4.72	355.98
9	170	999.59	16.21	12.27	5.07	2.23
10	180	998.42	16.07	12.08	5.17	3.82
11	190	997.24	15.93	11.91	5.64	7.98
12	200	996.06	15.83	11.83	7.22	2.53
13	210	994.88	15.62	11.76	7.47	357.82
14	220	993.70	15.51	11.78	7.37	353.39
15	230	992.53	15.42	11.81	7.39	348.93
16	240	991.35	15.31	11.87	7.34	348.47
17	250	990.18	15.22	11.94	6.99	1.89

Thus, editing of obviously bad data and slight smoothing of the resulting pressure profile are apparently justified.

Finally, the 3-5s lag constants of the temperature and humidity sensors allow resolution of the sharp temperature and humidity gradients just above cloud top. To preserve these sharp gradients, smoothing of the temperature and humidity data should be avoided.

With these points in mind we have proceeded to produce Level II thermodynamic data in the following manner. After editing obviously bad data we have fit a cubic spline interpolation function to the raw data pairs (t_i, p_i) , $i = 1, 2, \dots$, to obtain the continuous function $p(t)$. Since noise in the aneroid sensor occasionally causes $p(t)$ to be nonmonotonic, we have sampled $p(t)$ at 3 sec intervals and then applied an eleven point filter with the weights $(-1, -5, -5, 20, 70, 98, 70, 20, -5, -5, -1)/256$. This filter has the monotone spectral response shown in Fig. 16. It effectively removes oscillations with periods shorter than 18 seconds. More detail on this filter can be found in Hamming (1983, pages 143-144). We next perform a cubic spline fit to the filtered pressure data, thus obtaining the monotonic continuous function $\bar{p}(t)$, which is then evaluated at the original t_i to

produce \bar{p}_i . We then convert filtered pressure data into height data using the discrete hydrostatic relation

$$z_i - z_{i-1} + \frac{R}{2g} (T(t_i) + T(t_{i-1})) \ln \left(\frac{\bar{p}(t_{i-1})}{\bar{p}(t_i)} \right) \quad (14)$$

This upward integration commences at the 97m launch elevation. A cubic spline is then fit to the (z_i, t_i) data to obtain the continuous function $t(z)$. From the continuous function $t(z)$, we then find t_j corresponding to equally spaced 10m intervals in z_j . We then linearly interpolate temperature and relative humidity from the nearest two times to obtain data at equally spaced intervals of height.

From the pressure \bar{p} , temperature T and relative humidity U we could now compute derived quantities such as dew point temperature T_d , water vapor mixing ratio q , saturation water vapor mixing ratio q_s , potential temperature θ , equivalent potential temperature θ_e and saturation equivalent potential temperature θ_{es} . To guarantee a manageable size of the Level II data set, we have included only T_d . A sample from the Level II data set is shown in Table 10. The computation of T_d and the other derived fields (which the user must compute) are described below.

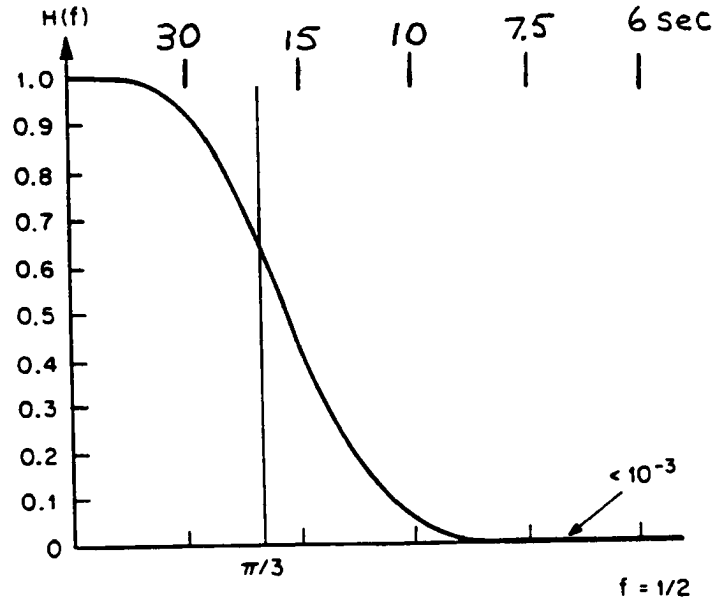


Figure 16: Monotone spectral response of the filter used in sections 5.11 and 5.12 for the processing of the thermodynamic and wind data. The lower abscissa is labeled in frequency (where $f = 1/2$ corresponds to one-half oscillation per data point) and the upper abscissa in period (seconds) assuming a 3 second interval between data points. The filter effectively removes oscillations with periods shorter than 18 seconds.

By first computing the saturation vapor pressure $e_s(T)$ from

$$e_s(T) = 6.112 \exp \left(\frac{17.67(T-273.15)}{T-29.65} \right) \quad (15)$$

(where $e_s(T)$ is in millibars and T in Kelvin) and the actual vapor pressure e from

$$e = U e_s(T), \quad (16)$$

we can compute the water vapor mixing ratio q and the saturation water vapor mixing ratio q_s from

$$q = \frac{\epsilon e}{p - e} \quad (17)$$

and

$$q_s = \frac{\epsilon e_s(T)}{p - e_s(T)}, \quad (18)$$

where $\epsilon = 0.622$ is the ratio of the molecular weight of water vapor to the molecular weight of dry air. Equation (15) is Bolton's (1980) fit to the highly accurate (0.005%) formula of Wexler (1976). The accuracy of (15) is 0.1%. Since the dew point temperature T_d is defined by $e_s(T_d) = e$, we can rearrange (15) to obtain

$$T_d = 273.15 + \frac{243.5 \ln(e/6.112)}{17.67 - \ln(e/6.112)}, \quad (19)$$

which allows explicit determination of T_d from the vapor pressure e .

We can next compute the potential temperature, equivalent potential temperature and the saturation equivalent potential temperature from

$$\theta = T(p_0/p)^\kappa \quad (20)$$

$$\theta_e = \theta \exp(2.67 q/T_s), \quad (21)$$

and

$$\theta_{es} = \theta \exp(2.67 q_s/T), \quad (22)$$

where the saturation level temperature T_s is given by

$$T_s = \frac{1}{\frac{1}{T-55} - \frac{\ln(U/100)}{2840}} + 55. \quad (23)$$

The constants in (21) and (22) were suggested by Betts (1982) and those in (23) by Bolton (1980).

5.12 Analysis of the wind data

The underlying principle in obtaining winds from balloon tracking is that the horizontal wind velocity is equal to the velocity of the vertical projection of the balloon onto the spherical surface through which the balloon is rising. It is obvious that this principle is not exact, since the balloon is rising through a vertically sheared wind field and requires some time to accelerate or decelerate and thus match its velocity with that of the surrounding air. In this sense, wind measurements by balloon tracking have lags just as the temperature and humidity measurements discussed in section 5.11. When attempting to obtain high vertical resolution in wind observations, a second topic of concern is self-induced balloon motions, i.e., a tendency for balloons to snake their way through still air rather than rising straight up. These two issues, which can be lumped under the general question of how well balloons follow the flow, are discussed in the following two subsections. In the third subsection we discuss the advantages and disadvantages of radiotheodolite systems. When computing winds from radiotheodolite measurements, the issue of the effects of the earth's curvature is also important. This subject is discussed in the fourth subsection.

5.121 Inertial lag of the balloon

Consider a spherical balloon filled with hydrogen or helium so that it has lift $L = \rho Vg$, where ρ is the air density and V the balloon volume. Suspended below the balloon is a radiosonde, with the whole structure (balloon, gas, suspension line, radiosonde) having mass m and associated downward gravitational force mg . In still air the balloon tends to rise straight up with an associated downward drag force (neglecting the drag on the sonde) equal to $1/2 c_D \rho A w^2$, where c_D is the drag coefficient (typically about 0.4), A is the cross-sectional area of the balloon, and w is the balloon rise rate (typically about $5ms^{-1}$). The force balance for steady vertical ascent is then

$$1/2 c_D \rho A w^2 + mg = \rho V g. \quad (24)$$

Typical values of the drag force, weight and lift are 8, 5 and 13 Newtons respectively.

If the balloon rises through a sheared flow, the drag force is not exactly vertical but is in a direction opposite to the motion of the balloon relative to the moving air. The horizontal component of this drag force will accelerate or decelerate the balloon so that its velocity becomes closer to that of the air. The formal solution of this problem has been given by Perkins (1952), who concludes that the measured wind is a weighted average of the actual wind over a layer of thickness.

$$d = \frac{6m}{c_D \rho A} \quad (25)$$

Retaining (24) as the approximate force balance in the vertical, we can eliminate $c_D \rho A$ between (24) and (25) to obtain

$$d = \frac{3w^2}{g(\gamma - 1)} \quad (26)$$

where $\gamma = L/(mg)$ is the lift ratio. Note that $\gamma > 1$ is a necessary condition for the balloon to rise. For rise rates $3 < w < 6 \text{ ms}^{-1}$ and lift ratios $2 < \gamma < 3$, (26) yields $1 < d < 11 \text{ m}$. Since the sampling interval is approximately 10m, we can assume that there are negligible lag effects in the wind data. In other words, it can be safely assumed that the balloon is moving with the wind, with the qualifications discussed in the next subsection.

5.122 Self-induced balloon motions

McVehil et al. (1965) tracked one-meter and two-meter diameter metalized spherical balloons with a pulsed Doppler radar, which yielded high vertical resolution soundings of the radial (i.e., along the radar beam) velocity component of the balloon. For a two-meter diameter balloon rising at 8 ms^{-1} , regular oscillations with a vertical wavelength of 30 to 80 m were found. Such oscillations may be associated with turbulence in the boundary layer flow about the balloon. Experiments with one-meter diameter balloons yielded qualitatively similar oscillations with a vertical wavelength of approximately 15 m. McVehil et al. concluded that one-meter and two-meter diameter balloons do not move entirely with the wind but have spurious oscillatory components that are aerodynamically induced. The wind speed errors associated with these spurious oscillations are expected to be approximately 1 to 2.5 ms^{-1} .

Self-induced motions of flexible rubber balloons and rigid mylar balloons were also observed by Murrow and Henry (1965) in a large dirigible hangar at Lakehurst, NJ. The balloons were released in the still air of the hangar and the deviations from perfectly vertical ascent measured with phototheodolites. The root-mean-square horizontal velocity was proportional to the vertical terminal velocity. For smooth rigid spheres of two-meter diameter the rms horizontal velocity was approximately one-half the vertical terminal velocity. Scoggins (1965) found that the use of roughened spheres (i.e., spheres with 90 or 270 cup-like structures protruding from the

surface) reduced the amplitude of the aerodynamically induced motion.

Two brands of flexible rubber balloons were used in ASTEX. We believe these balloons produce self-induced motions, although the radiosonde train below the balloon probably reduces the effect somewhat. Thus, we suggest that it may be misleading to examine the wind data at vertical resolutions higher than approximately 100m.

5.123 Advantages and disadvantages of radiotheodolite systems

The measurements used in making upper air wind computations through balloon tracking by radiotheodolite or radar include the azimuth angle (α), the elevation angle (ϵ), the balloon height (z), and the slant range (r), all as functions of time. Given α , only two of the remaining three variables (ϵ, z, r) are required for wind computation. Thus, de Jong (1958) has arranged wind observations into three classes—those using (ϵ, z), those using (ϵ, r), and those using (z, r). Radiotheodolite systems fall into the (ϵ, z) class, while radar systems measuring elevation and slant range fall into any class and radar systems measuring slant range but not elevation fall into either or both of the (ϵ, r) and (z, r) classes. By performing an error analysis, de Jong has concluded that no one class is always superior and that each class has its advantages in certain ranges of the variables. The (ϵ, z) class is best when balloon distances are not too large and elevation angles are not too small. When the balloon is a large distance away, the (z, r) class is most suitable and the (ϵ, z) class least suitable. In addition, when the balloon instantly moves in the direction of observation, the wind speed errors maximize, while when the balloon instantly moves perpendicular to the direction of observation these same errors minimize.

In summary, the use of a radiotheodolite system for boundary layer wind measurements as required by ASTEX is a good choice. In cases of strong unidirectional flow, when the balloon drifts directly away at low elevation angles, the upper level winds are less reliable. However, it should be noted that tropospheric winds are also available from a 400 MHz wind profiler on Porto Santo.

5.124 Effects of the earth's curvature on wind computations

When pibal observations are used to compute winds, the distances from the theodolite are not large and it is acceptable to neglect the curvature of the earth. Since the advent of the AN/GMD-1 system in the early 1950's it has become common to track balloons to heights above 30km and out to ranges exceeding 200km, with elevation angles as low as 6 degrees. For such cases it is important to include

the effects of the earth's curvature (Gustafson 1954, Clem et al. 1954, Kessler 1954).

Consider a cross section which contains the center of the earth (C), the radiotheodolite observation site (O) and the balloon position (B), as shown in Fig. 17 (after Clem et al. 1954). In this figure $z-z_s$ is the height of the balloon above the observation site (which is at height z_s above sea level), ϵ the elevation angle, ϕ the angle subtended at the center of the earth, a the radius of the earth (assumed spherical), D the great circle distance along AB (which is concentric with OS), d the horizontal distance to the position of the balloon projected onto the tangent plane OP.

Since OPB and CGB are right triangles, we have $h/d = \tan \epsilon$, $d/(a+z-z_s) = \sin \phi$ and $d/(a+h) = \tan \phi$. Using the first of these to eliminate h from the third, and then using the second to eliminate d , we obtain

$$\cos \phi \cos \epsilon - \sin \phi \sin \epsilon = \frac{a \cos \epsilon}{a + z - z_s}. \quad (27)$$

Since the left hand side of (27) can be written as $\cos(\phi + \epsilon)$, we can solve for ϕ to obtain

$$\phi = \cos^{-1} \left(\frac{a \cos \epsilon}{a + z - z_s} \right) - \epsilon \quad (28)$$

The great circle distance D is then given by

$$D = (a + z - z_s) \phi. \quad (29)$$

The velocity components v_r and v_α are given by

$$v_r = \dot{D}, \quad (30)$$

$$v_\alpha = \dot{\alpha}(a+z-z_s) \sin \phi, \quad (31)$$

where the dot denotes a time derivative. The eastward component v and the northward component u are then obtained from v_r and v_α by

$$u = v_r \sin \alpha + v_\alpha \cos \alpha, \quad (32)$$

$$v = v_r \cos \alpha - v_\alpha \sin \alpha. \quad (33)$$

Wind speed and wind direction are easily obtained from either v_r , v_α or u , v .

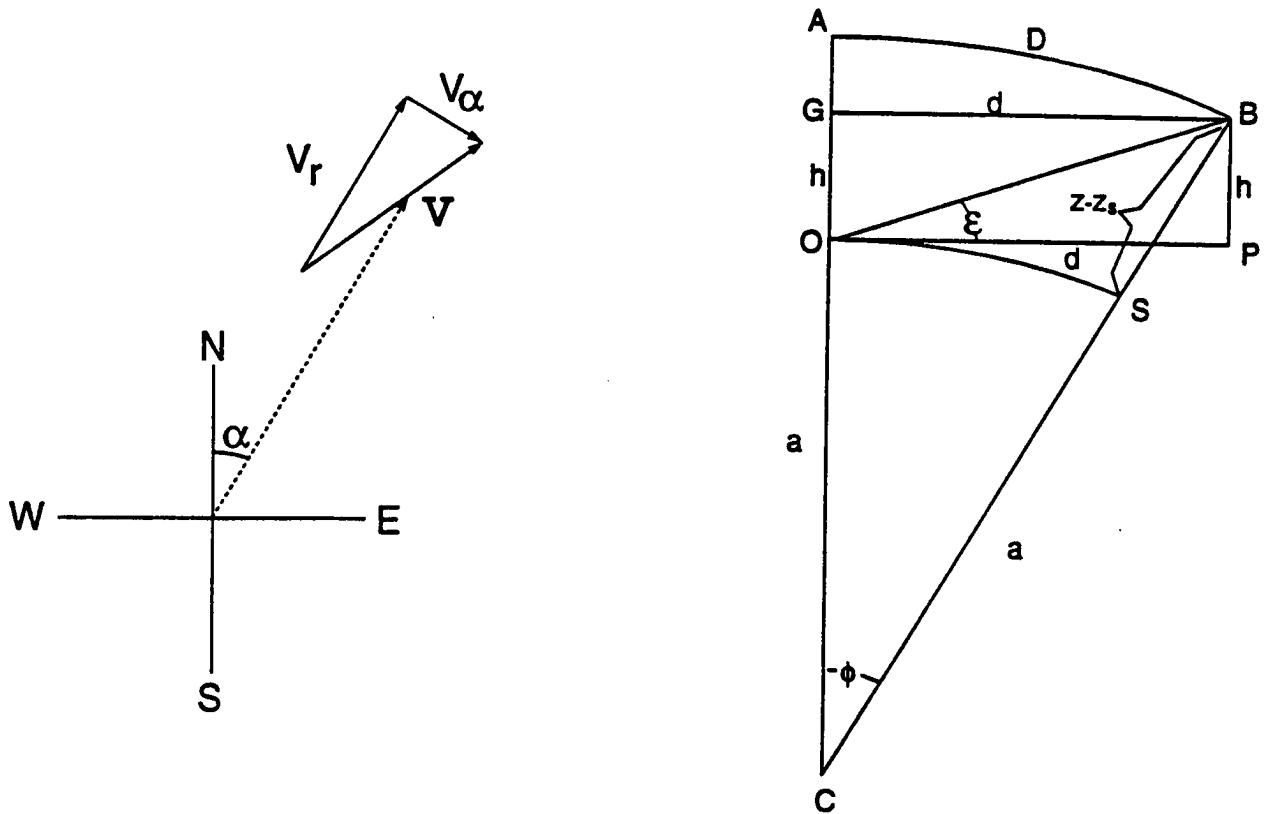


Figure 17: The left diagram shows the balloon position (dashed vector) at azimuth α . The wind at this balloon position is v , which has horizontal components v_r in the radial direction and v_α in the tangential direction. The right diagram is a vertical plane through the center of the earth (C), the radiotheodolite observation site (O) and the balloon position (B) (after Clem et al. 1954). Here $z - z_s$ is height of the balloon above the observation site, ϵ the elevation angle, ϕ the angle subtended at the center of the earth, a the radius of the earth (assumed spherical), D the great circle distance along AB (which is concentric with OS), d the horizontal distance to the position of the balloon projected onto the tangent plane OP.

We can now summarize our Level II wind calculations as follows. We first fit spline interpolation functions to the raw azimuth and elevation angles. We then evaluate the spline functions at equally spaced 3 second intervals. This data is then filtered with the same eleven-point filter described in the previous section, which produces

$$\bar{\alpha}(t) \quad \text{and} \quad \bar{\epsilon}(t). \quad \text{From the time series } \bar{\epsilon}(t) \quad \text{and} \quad z(t)$$

we compute the new time series $\phi(t)$ and $D(t)$ using (28) and (29). We then perform a spline fit to $D(t)$, which gives, as a

by-product, $\dot{D}(t)$. The quantities $\dot{D}(t)$ and $\dot{\alpha}(t)$ are then used in (30) and (31) to compute v_r and v_α , after which wind speed and direction are computed.

Due to problems in measuring the wind discussed earlier in this section, some undesirable oscillations are present in the wind data. To remove these oscillations the AIR software filters the wind data by taking layer averages of the vector wind components u and v . The length of this layer average is a function of the balloon height as follows:

30	sec	up to	2500m	AGL
45	sec	up to	5000m	AGL
60	sec	up to	7500m	AGL
75	sec	up to	10km	AGL
90	sec	up to	15km	AGL
105	sec	up to	20km	AGL
120	sec	above	20km	AGL

This filtering is present in the Level I analysis. In the Level II analysis no filtering of u and v is done so that considerable noise is still present in the Level II wind data. Thus, depending on their purposes, users of this data must decide what type of additional smoothing should be applied.

5.13 Atmospheric sounding data

Each of the soundings was processed by the techniques described in sections 5.21 and 5.31. Graphical depictions of the rawinsonde data are presented in the CSU Atmospheric Science Paper No. 512, (Schubert, et al., 1992). Appendix 1 presents a listing of all rawinsonde ascents conducted from the island of Porto Santo during the field phase of ASTEX.

The Level I and Level II data described in this report are available via anonymous ftp from the machine *rossby.atmos.colostate.edu* (IP address 129.82.107.97). The Level I data totals 39.1 megabytes and the Level II data 23.8 megabytes. Detailed instructions on how to obtain either the Level I or Level II data are contained in the file */dist/astex/sonde/README*. Any problems with the data or difficulties in accessing it should be reported to Paul Ciesielski at the following email address: *paulc@einstein.atmos.colostate.edu*. The data are also available through the NASA ASTEX archive.

REFERENCES

- Albrecht, B. A., C. W. Fairall, D. W. Thomson, A. B. White, J. B. Snider and W. H. Schubert, 1990: Surface-based remote sensing of the observed and the adiabatic liquid water content of stratocumulus clouds. *Geophysical Research Letters*, **17**, 89-92.
- Ballard, L. J., R. H. Swansborough and R. Johnson, 1983: Detailed specification for a pilot wind power scheme on Porto Santo. ERA Report No. 83-0187. ERA Technology Ltd, Cleeve Road, Leatherhead, Surrey KT22 7SA, England.
- Betts, A. K., 1982: Saturation point analysis of moist convective overturning. *J. Atmos. Sci.*, **39**, 1484-1505.
- Bolton, D., 1980: The computation of equivalent potential temperature. *Mon. Wea. Rev.*, **108**, 1046-1053.
- Clem, L. H., D. Colson and L. P. Harrison, 1954: Corrections of upper-level wind computations for effect of earth's curvature. *Bull. Amer. Meteor. Soc.*, **35**, 357--362.
- de Jong, H. M., 1958: Errors in upper-level wind computations. *J. Meteor.*, **15**, 131--137.
- FIRE Project Office, 1992: ASTEX Operations Plan. Available from David S. McDougal, FIRE Project Manager, Mail Stop 483, NASA Langley Research Center, Hampton, VA 23665-5225.
- Gustafson, A. F., 1954: The error in rawin computations due to neglecting the earth's curvature. *Bull. Amer. Meteor. Soc.*, **35**, 295-300.
- Hamming, R. W., 1983: *Digital Filters*, Second Edition. Prentice-Hall, Englewood Cliffs, New Jersey, 257 pp.
- Kessler, E., 1954: Curvature corrections for radiowind reports. *Bull. Amer. Meteor. Soc.*, **35**, 328-330.
- Kuo, H.-C., and W. H. Schubert, 1988: Stability of cloud-topped boundary layers. *Quart. J. Roy. Meteor. Soc.*, **114**, 887-916.
- McVehil, G. E., R. J. Pilié and G. A. Ziggrossi, 1965: Some measurements of balloon motions with Doppler radar. *J. Appl. Meteor.*, **4**, 146-148.
- Murrow, H. N., and R. M. Henry, 1965: Self-induced balloon motions. *J. Appl. Meteor.*, **4**, 131-138.
- Perkins, D. T., 1952: The response of balloons to the wind. *Bull. Amer. Meteor. Soc.*, **33**, 135-139.

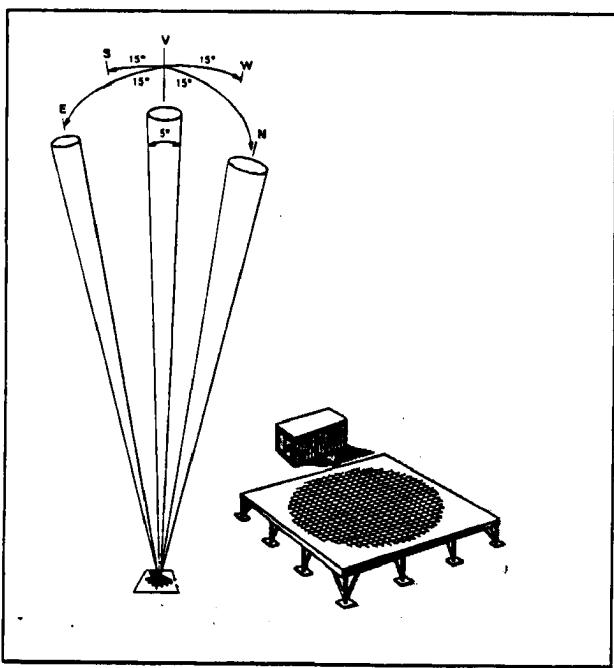
Randall, D. A., 1980: Conditional instability of the first kind upside-down. *J. Atmos. Sci.*, **37**, 125-130.

Schubert, W. H., 1992: Analysis of sounding data from Porto Santo Island during ASTEX. Colorado State University, Department of Atmospheric Science, Report No. 512, 96 pgs.

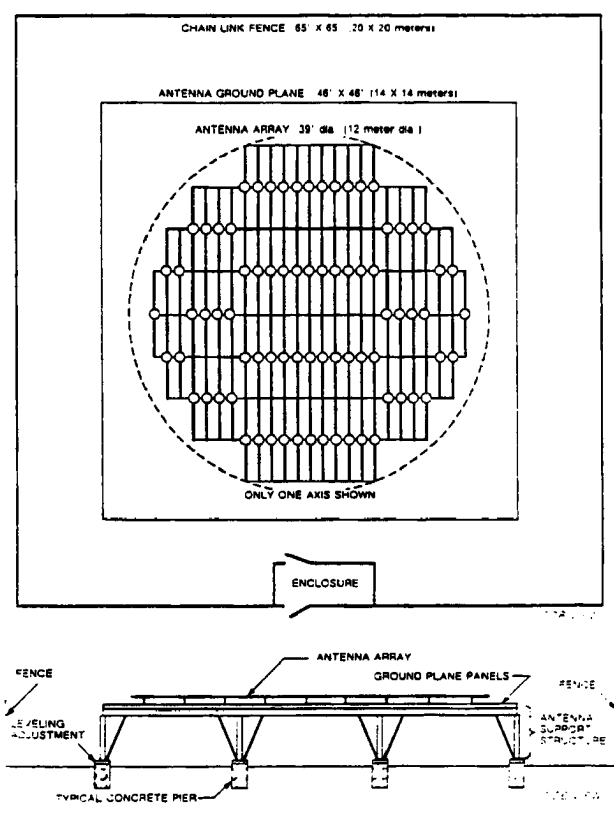
Scoggins, J. R., 1965: Spherical balloon wind sensor behavior. *J. Appl. Meteor.*, **4**, 139-145.

Wexler, A., 1976: Vapor pressure formulation for water in range 0 to 100°C. A revision. *J. Res. Nat. Bur. Stand.*, **80A**, 775--785.

5.2 Model 400 Wind Profiler



Typical beam configuration in wind profiling consists of three beams: one vertical, and two tilted 15° from the zenith (to the east and north, for example). Under some circumstances, two additional beams are needed (such as to the south and west).



Typical Model 400 wind profiler site.

Figure 18: Wind profiler system

Where, V_{re} , V_{rn} , and V_{rz} are radial velocities measured in the east, north, and zenith directions, respectively. U, V are east-west, north-south components of horizontal wind, respectively; W is the vertical velocity.

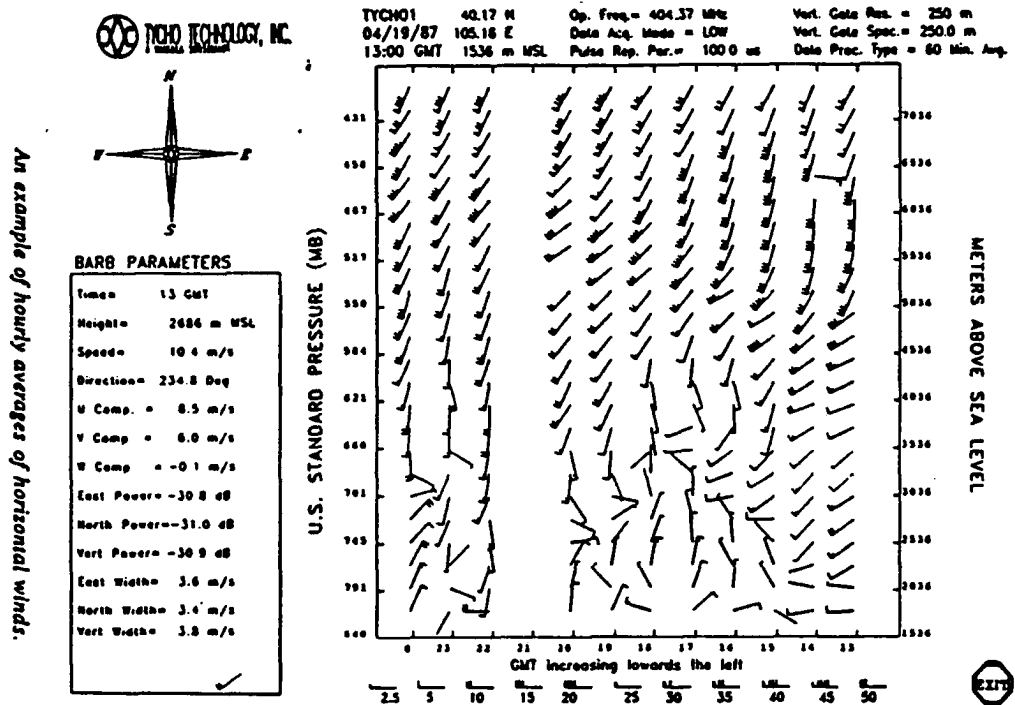


Figure 21: Hourly averaged wind profile

5.23 Specifications

5.231 Wind Profiler Site Location:

Porto Santo, Portugal: Elevation: 97m above sea level; Latitude: 33° 5' 2" N Longitude: 16° 20' 49" W

5.232 The Wind Profiler Parameters:

Table 11 lists the operator selected parameters which determine the operating characteristics of the wind profiler. Values assigned to these parameters are given in the Appendix 7. Here, we should

mention that, during the whole FIRE period, we used five beams. So the data time cycle was about 10 minutes plus one minute to transfer the spectrum to an optical disk archive.

5.233 Height Coverage and Resolution:

The wind profiler has high and low modes. The low mode covers the height from 500m above ground level (AGL) to 9.25km AGL with height resolution of 250m. The high mode covers the height from 7.50km AGL to about 16.25km AGL with a height resolution of 1000m.

Title:
mode__1_26_Nov_1991_12:32:44_Gate_24_Height_xxxxx/

Byte1--4: 'mode'
Byte6--7:mode number 1--10
Byte9,10:day
Byte12-14:month
Byte16-19:year
Byte21-28:time
Byte30-33:'Gate'
Byte35-36:gate number 1--36
Byte38-43:'Height'
Byte45-49:height in digital format
Byte50:return

After above title, a 256x4 byte binary array is saved. This array is the spectrum for the mode and gate specified by the title. In each file, we have 360 arrays.

5.2412 Processed data

The processed data are derived from the Tycho processing program. They include all of the moments data: signal power, radial velocity and speed variance. The data have been saved in the TK50 tapes with the following file format:

yymmdd_hhmmss.new (covers the every cycle data in one hour)
yymmdd_hhmmss.pro (covers the data which has been hourly averaged)

and,

yymmddhh.ard (cycle data after quality control)
yymmddhh.arc (hourly-averaged data after quality control)

5.242 Accessing of the Data

As mentioned above, spectra data are archived at CSU on optical disk and moment data on TK 50 and exabyte tapes.

References:

Cox, et al., 1992: CSU FIRE II Cirrus Field Experiment: Description of Field Deployment Phase. Colorado State University, Department of Atmospheric Science, Paper No. 506, 55 pgs.

Peterson, V. L., 1988: Wind Profiling - The History, Principles, and Applications of Clear-air Doppler Radar. Tycho Technology, Inc.

Tycho Technology, Inc., 1989: Model 400s Wind Profiler Software User's Manual.

van de Kamp, D. W., 1988: Wind Profiler Training Manual #1-Principles of Wind Profiler Operation. NOAA Documents Developed for the National Weather Service Office of Meteorology.

5.3 Radio Acoustic Sounding System

5.31 Instrument Description

The Radio Acoustic Sounding System (RASS) is used to acquire temperature profiles of the boundary layer. There are several methods available to use RASS all of which involve introducing an audio signal into the atmosphere and tracking the speed of the acoustic wavefronts using a sensitive Doppler RADAR. By adjusting the audio frequency such that the acoustic wavelength is half that of the transmitted radio frequency (i.e. satisfies the Bragg condition) and by using a wind profile RADAR (or wind profiler), the temperature at a given height can be obtained from the equation (Nalbandyan, O. G., 1977)

$$C_a - 20.047\sqrt{T_v} + v_w \quad (m/s) \quad (34)$$

where C_a is the speed of sound, T_v is virtual temperature in degrees Kelvin and v_w is the wind velocity component parallel to acoustic wave propagation.

The RASS method used presently at CSU is the Receiver Offset Method. After a user-determined number of profiler cycles, the intermediate frequency in the wind profiler's receiver is offset via a single-sideband up-converter, (Strauch, R. G., 1988). The offset causes the baseband of the receiver's discrete-time filter to be shifted to the audio frequency used by RASS.

Shortly after the offset is applied and before the RASS mode begins, a separate oscillator sweeps through a narrow band of audio frequencies selected according to expected air temperatures. This signal is then amplified and broadcast over four loudspeakers which are placed approximately 10 meters away from and encircling the RADAR antenna. When the Bragg condition is satisfied, the strongest signals at the receiver for each range gate will be those of acoustic wavefronts traveling at the velocities corresponding to the temperatures at those altitudes. The Receiver Offset Method was the RASS procedure employed during the ASTEX experiment in Porto Santo, Portugal.

5.32 Specifications

5.321 Electromagnetic

Radar	Tycho DORA 400S Wind Profiler
Transmit Frequency	404.37 MHz
Radiated Power	40 kW (peak)
Beamwidth	5 degrees
Antenna Type	Phased Array Coaxial Collinear Dipoles
Antenna Diameter	12 meters

5.322 Acoustic

Transducer Type	Folded Horn with Compression Driver
Transducer Sensitivity	105 dB SPL (1W/1m)
Radiated Power	75 Watts (average)
Beamwidth	110 degrees horizontal 130 degrees vertical

5.323 Data Summary

All data collected by the wind profiler are stored in two formats - as processed spectral moment data and as raw spectra. Temperature profiles are determined from the spectra (see Figure 22) by the equation

$$T_v = \left(\frac{v_{app} - v_{offs}}{20.047} \right)^2 \quad (K) \quad (35)$$

where T_v is virtual temperature and v_{app} is the apparent velocity reported by the profiler. The offset velocity, v_{offs} , results from the offset frequency, f_{offs} , and is calculated from

$$v_{offs} = \lambda_{emr} / 2 f_{offs} \quad (m/s) \quad (36)$$

where λ_{em} is the wavelength of the electromagnetic radiation.

During the FIRE II experiment, RASS data were collected every sixth profiler cycle during normal daylight operating periods. During intensive data collection intervals or during maintenance, RASS may have been activated more or less often.

References:

- Cox, et al., 1992: CSU FIRE II Cirrus Field Experiment: Description of Field Deployment Phase. Colorado State University, Department of Atmospheric Science, Paper No. 506, 55 pgs.
- Nalbandyan, O. G., 1977. The Theory of Radioacoustic Sensing of the Atmosphere. *Izvestiya, Atmospheric and Ocean Physics*, 13, No. 3.
- Strauch, R. G., K. P. Moran, P. T. May, A. J. Bedard, W. L. Ecklund, 1988. RASS Temperature Sounding Techniques. NOAA Technical Memorandum ERL WPL-158.

911120_221742.spc

MODE: 1

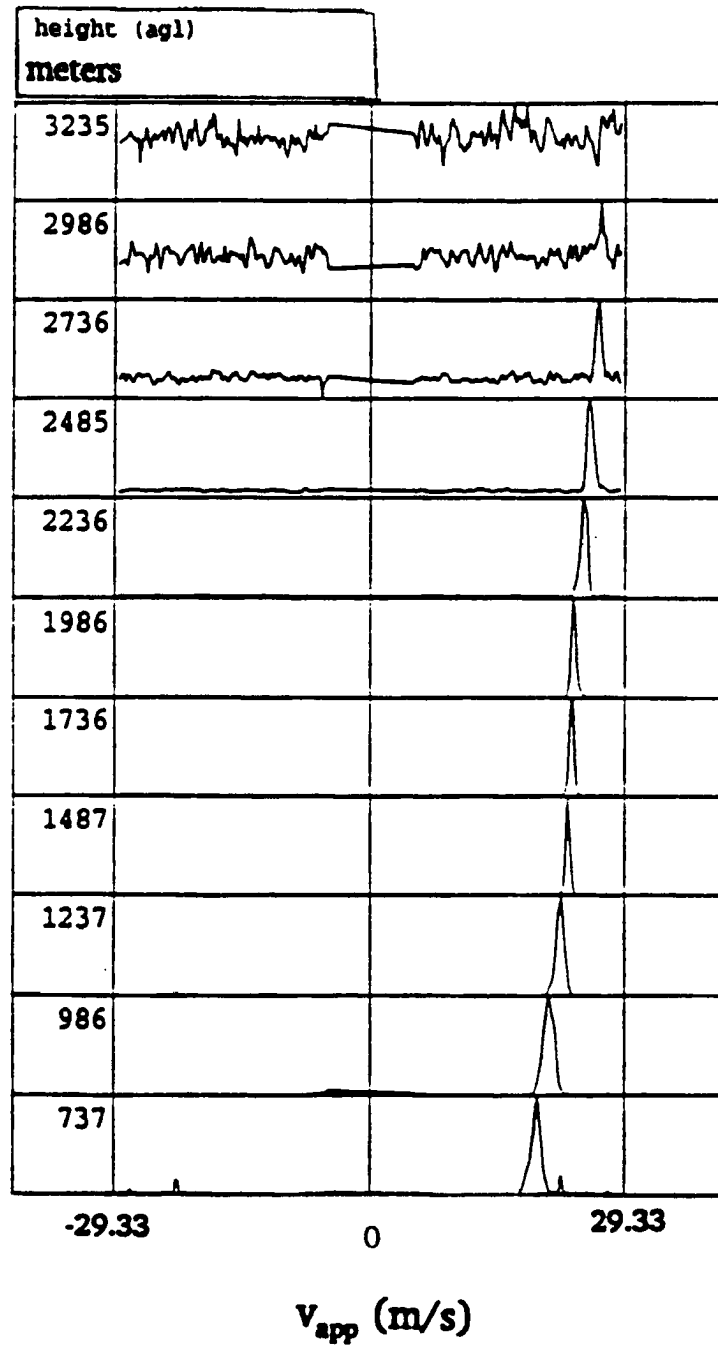


Figure 22: Sample RASS spectra (colder temperatures to the right).

6.0 Cloud Measurements

6.1 Laser Ceilometer

6.11 Instrument Description

The Belfort Laser Ceilometer used at the Porto Santo site of the 1992 ASTEX experiment is an active LIDAR system which employs a laser fired into a vertically pointing 10 inch optical system to detect cloud base height.

The ceilometer utilizes a 20 watt near-infrared Gallium-Arsenide laser operating at a wavelength of .91 microns. It employs 1024 range gates which yield a vertical resolution of 25 feet up to a maximum range of 25,600 feet. The fields of view of the transmitter and receiver are approximately 1 degree.

The time interval between consecutive ceiling observations may be set between 30 seconds and 12 minutes; for each ceiling observation, the ceilometer goes through a cycle of environmental-engineering measurements, the actual sampling interval, an analysis period and data transmission period. The cycle begins by sampling all 1024 range gates at 1 KHz for three consecutive cycles without firing the laser. These three cycles are combined to provide a "noise level figure of merit" for each range gate. Next the laser is fired 5120 times and the reflected signal is sampled for each range gate. On each of the 5120 scans, for each range gate, the signal is compared with the appropriate noise level value for that gate. Depending on whether the received signal is above, below, or within the noise level band, an integer value of 1, -1 or zero, respectively, is assigned to that gate. These assigned integers are then summed for each gate and thus represent a modified histogram of "counts" versus height. This histogram becomes the basic digital output product of the ceilometer. A firmware peak-location algorithm is then applied to this product to produce a first order estimate of the ceiling. The histogram, the first order estimate of ceiling, and some engineering data are then provided via an RS 232 port to a local 386 class personal computer where the data are archived. In this form, the data provide reliable ceiling estimates, however because the firmware does not account for atmospheric attenuation of the signal, one should not rely upon this product for parameters such as cloud amount or extinction characteristics of the cloud.

The discretized digital counts which represent the signal return for each range gate are available in ASCII files described in the next section. The cloud base value deduced by firmware, which also differentiates between "cloud" and "clear" in real-time has been found to

8.0 NOAA/WPL Compact Doppler Lidar

A new compact Doppler lidar, designed specifically for boundary layer studies, was operated for the first time on Porto Santo. Intended for installation in a seatainer, the system was assembled and operated in a temporary wood building during ASTEX. Ultimately, it is hoped that the lidar will be deployed on both ship and aircraft platforms for boundary layer studies.

The lidar operates in the thermal infrared at wavelengths in the 9-11 μm spectral region. It employs a carbon dioxide, Q-switched laser, followed by an optical amplifier to produce pulses of a few mJ at pulse rates of up to 3 kHz. Eventually, it is hoped that pulse energy can be boosted to 10-20 mJ, increasing range and boosting sensitivity. The oscillator-amplifier design of the lidar provides high optical stability and extremely pure output pulses; this should enable wind measurements to be obtained with accuracies of 10 cm s^{-1} or better.

At Porto Santo, the lidar was operated with a new, computer-controlled scanner and a new, untested signal processing system. Both caused some difficulties during the experiment. Primary data products from Porto Santo will be episodic observations of winds in the subcloud region, including vertical velocity profiles and statistics, horizontal wind profiles, and profiles of turbulent kinetic energy and momentum flux. Also potentially available will be estimates of droplet mode radius at cloud base (calibration difficulties may preclude this observation.)

References:

Pearson, G. N., B. J. Rye, and R. M. Hardesty, 1990: Design of a high pulse repetition rate CO_2 Doppler lidar for atmospheric monitoring. Proceedings, High Power Lasers and Optical Computing Conference, Los Angeles, CA, 14-19 January, 1990, SPIE, Bellingham, WA 1222:142-153.

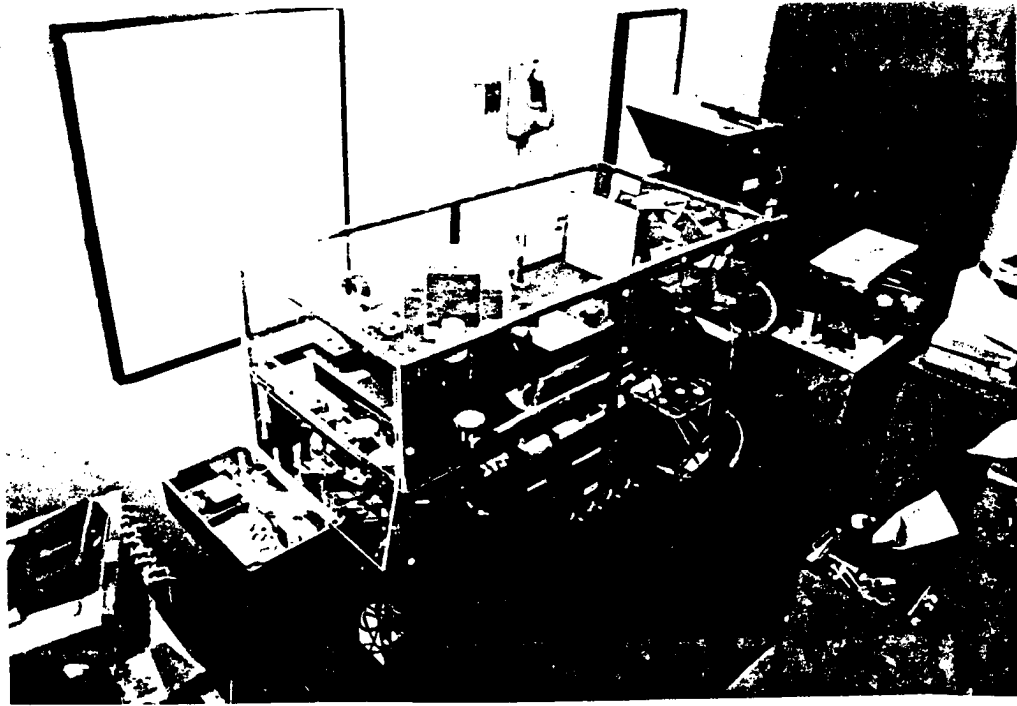


Figure 26: NOAA/WPL Doppler Lidar

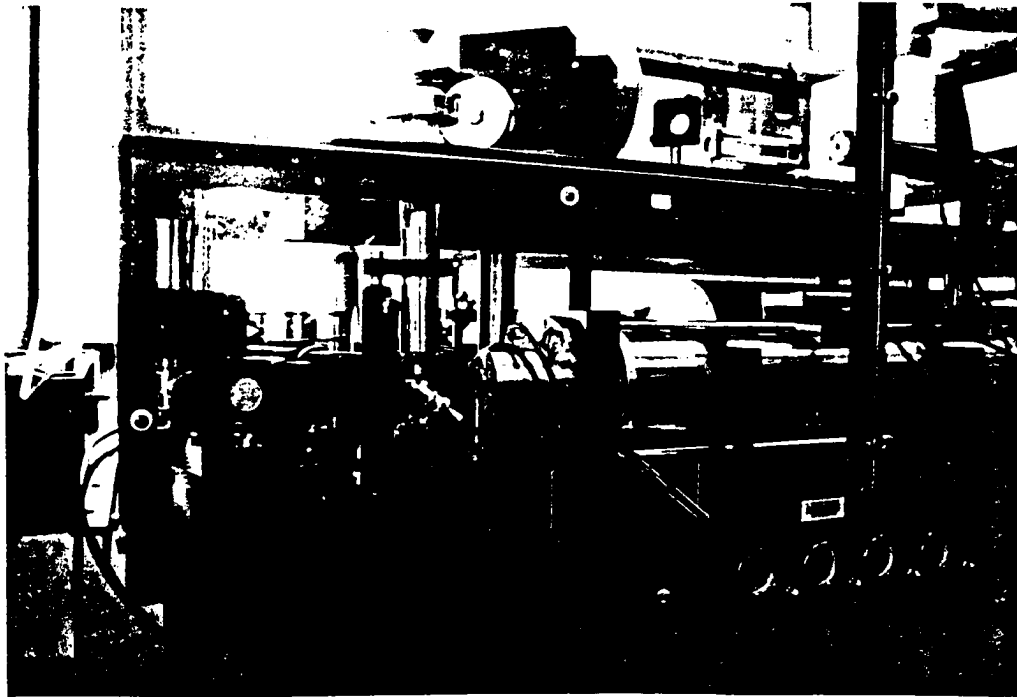


Figure 27: NOAA/WPL Doppler Lidar

9.0 NOAA/WPL Radiometers

A three channel microwave radiometer was deployed during ASTEX to measure the water vapor and liquid water path on a continuous basis. The 20.6 GHz channel is a water vapor absorption band while the 31.65 and the 90.0 GHz channels are in atmospheric windows and therefore, are influenced primarily by emission from the liquid phase. Table 14 gives the specifications for the 20.60 and 31.65 GHz radiometers. Table 15 lists the data products and anticipated accuracy of these products.

In addition to the microwave radiometers, NOAA/WPL deployed a modified PRT-5 radiometer with a spectral bandpass centered at 10.6 microns. This radiometer has a two degree field of view and was pointed at zenith. In addition to the 10.6 micron brightness temperature yielded by the PRT-6, broadband infrared irradiance data and hemispheric incident solar irradiance data were collected at the WPL site.

Table 14: Specifications for the WPL Microwave 2 Channel Radiometer

	Frequency (GHz)	
	20.60	31.65
Antenna		
3-dB beamwidth, deg	2.4	2.2
10-dB beamwidth, deg	4.2	4.4
Bandwidth, mHz	~ 500	~ 500
Noise temperature, K	675	875
Sensitivity at 1 s, K	0.10	0.12
Measured absolute accuracy (rms), K	0.97	0.94

Table 15: Data Products Derived from WPL Radiometer Measurements

Data Products	Estimated Accuracy
Integrated water vapor	± 1 mm
Integrated liquid water	10 percent
Cloud brightness @ 10.6 μm	± 1 K
Shortwave solar irradiance	TBD
Downwelling longwave irradiance	TBD

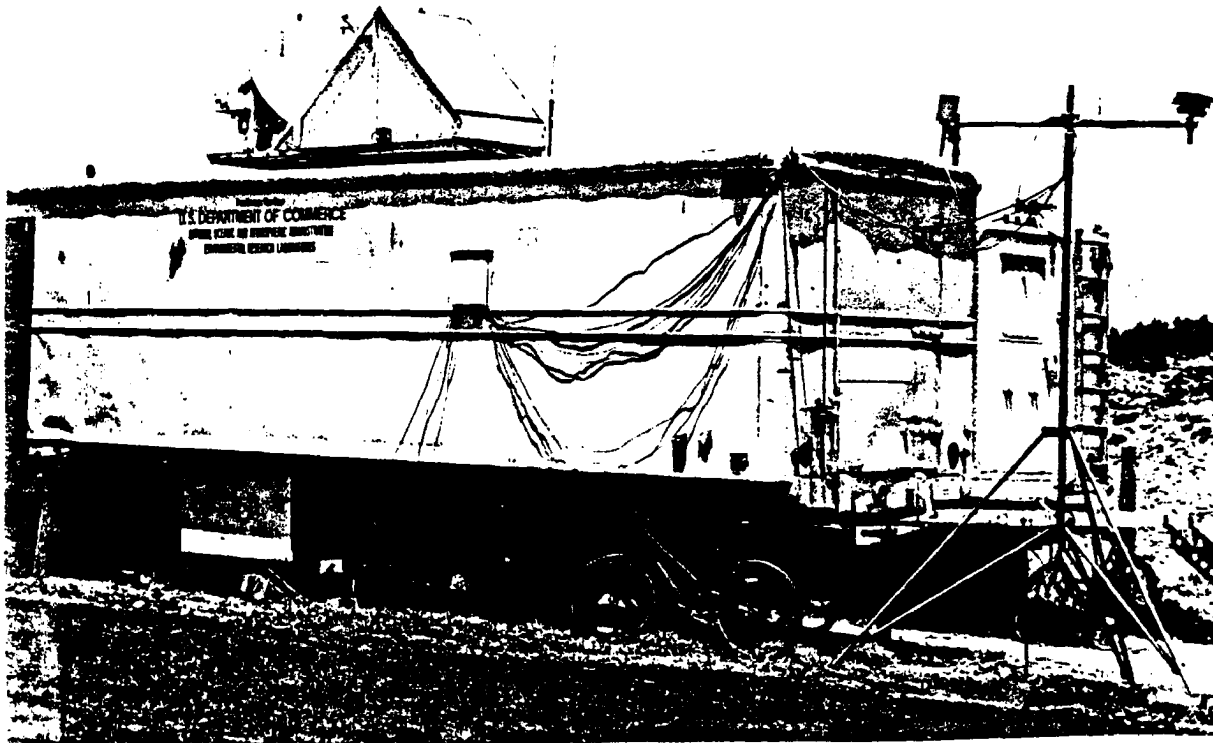


Figure 28: NOAA/ERL Microwave Radiometer

References:

- Hogg, D. C., F. O. Guiraud, J. B. Snider, M. T. Decker, and E. R. Westwater, 1983: A steerable dual-channel microwave radiometer for measurement of water vapor and liquid in the troposphere. *J. Climate Appl. Meteor.*, 22, 789-806.
- Snider, J. B., 1988: Verification of the accuracy of a network of water vapor radiometers. *Proc. IGARSS '88*, Edinburgh, Scotland, Sept. 13-16, 19-20.
- Snider, J. B., 1988: Radiometric observations of cloud liquid during FIRE. *Proc. IGARSS '88*, Edinburgh, Scotland, Sept. 13-16, 261-262.
- Westwater E. R. and F. O. Guiraud, 1980: Ground-based microwave radiometric retrieval of precipitable water vapor in the presence of clouds with high liquid water content, *Radio Science*, 15, 947-957.

10.0 Acknowledgements

An expedition as large as the CSU/NOAA Porto Santo deployment during ASTEX depends critically upon contributions from many people.

The authors wish to express their sincere appreciation to Ms. Melissa Tucker for her many contributions to the success of our ASTEX participation. Ms. Tucker supports our preparations for the field by arranging travel and accommodations, ordering equipment and monitoring budgets; she supports us while in the field by making our offices only a phone call away and acting on our behalf. Following the field experiment, her efforts are critical to reporting the scientific results derived from the field experiment. Her most direct contribution to this document is giving continuity and order to a multi-authored collection of critical information that will serve scientists studying the marine boundary layer and its cloud systems in the coming decade.

Paul Hein supported our ASTEX field activities from Fort Collins. On many occasions when we needed equipment and information from the US, Paul acted on our behalf. We thank him for his important contributions. We also thank the NOAA personnel who supported us, both at home and in the field.

Shipping equipment from Colorado to Porto Santo turned out to be much more complicated than we originally expected. The co-authors graciously extend our gratitude to Shelby Frisch from NOAA and to Mae Chu of INTERCONICS for their untiring efforts to insure that our five semi-trailers containing equipment arrived in Porto Santo in time for the experiment and back home again in Colorado intact.

During the experiment we received enthusiastic support from many citizens of Porto Santo. Most notably Jocelino Velosa and José Rosado assisted us many ways during the experiment. Without their assistance and that of their fellow Porto Santoans, we could not have met our expectations, neither scientifically nor logistically. One final thanks, to the residents of Camacha, who listened to our hourly RASS transmissions twenty-four hours a day without complaint; we doubt that there is a populated site in the whole of the US where this would be possible.

The authors also express their appreciation to Professor Steven Krueger from the University of Utah and to Sara Sousa, an undergraduate physics student from Funchal. Steve and Sara enthusiastically joined our grueling 24 hour rawinsonde shift schedule and thus made life much easier for the rest of us. They did this willingly and their sole rewards were the challenges and the joys of science.

Lastly, but not least, this experiment could not have taken place without the sustained support provided by Dr. Robert Abbey of ONR, Dr. Timothy Suttles of NASA and Dr. Michael Riches of DOE.

This research has been supported by The Office of Naval Research under Contract No. N00014-91-J-1422, P00002, National Aeronautics and Space Administration under Grant NAG 1-1146, The Department of Energy, Contract No. DE-FG02-90ER60970 and The National Science Foundation, Contract No. ATM-9113129.

11.0 List of Appendices

APPENDIX 1: RAWINSONDE ASCENT TIMES AND COMMENTS 78

**APPENDIX 2: INSTRUCTIONS FOR DISPLAYING CAMPBELL STATION
DATA IN SPECTRA CALC 87**

APPENDIX 3: PRT 6 CALIBRATION FROM INTERFEROMETER DATA .. 88

APPENDIX 4: CAMPBELL PRT6 DATA UPLOAD 89

APPENDIX 5: INTERFEROMETER OPERATION INSTRUCTIONS 91

APPENDIX 6: INTERFEROMETER SPECTRA REDUCTION 95

APPENDIX 7: CEILOMETER OPERATIONS PROCEDURES 97

**APPENDIX 8: FUNCTIONS OF CONTROL KEYS FOR THE CEILOMETER
HISTOGRAM PROGRAM 98**

APPENDIX 9: WIND PROFILER PARAMETERS 100

APPENDIX 1: RAWINSONDE ASCENT TIMES AND COMMENTS

Sounding Number	Date	Start Time (UTC)	End Time (UTC)	Maximum Altitude (km)	Observer's Comments
1	June 01	02:03	03:05	18.5	Good flight 70mb
2	June 01	04:56	05:35	12.0	Temperature and RH quit at 200mb just like #1.
3	June 01	08:04	09:16	22.0	1st sonde bad; good flight 40mb.
4	June 01	10:55	12:04	23.9	Lost AFC near 150mb to 30mb
5	June 01	14:00	14:56	17.8	Lost T and DP at 90mb
6	June 01	16:56	18:19	26.0	Good flight. Launch at 5:57. Reached 30mb at 7:15 Cut off at 21 mb.
7	June 01	23:01	23:46	13.5	Drizzle/15min(heavy). Good flight.
8	June 02	05:02	05:28	9.9	Lost track at launch until 895mb. Balloon burst at 280mb.
9	June 02	07:58	09:20	24.3	Launch at 8:58. Had to change pressure because it was a approx. 6 mb off.
10	June 02	10:57	12:19	23.9	no comment
11	June 02	16:57	18:18	22.6	Sonde in and out about 135mb due to 13 degree elev. and 120 azimuth (behind mountain).
12	June 02	20:08	21:12	19.5	Difficulty in getting signal strength large enough. Had to turn off and on again. Lost track at launch; used manual to acquire.
13	June 02	23:28	00:16	14.1	Flight good. Terminate to get report.
14	June 03	01:52	02:36	12.7	Lost at launch; got back at 990mb. Good flight, lost T, RH at 200mb.
15	June 03	04:57	05:20	6.1	Launch fine. Frequency shift: 1680-1671 prior to launch; 1671-1666 so quickly AFC missed. Balloon burst at 147mb.
16	June 03	07:57	09:09	22.1	no comment
17	June 03	11:02	12:14	20.9	1st balloon had holes
18	June 03	16:57	17:27	7.8	1st hydrogen balloon
19	June 03	23:05	00:15	20.7	Sonde seemed erratic went OK
20	June 04	05:00	06:13	21.3	Bad wind. Auto track stuck on hill. Good flight-50mb.
21	June 04	07:57	09:09	23.8	no comment
22	June 04	11:01	12:14	25.0	no comment

Sounding Number	Date	Start Time (UTC)	End Time (UTC)	Maximum Altitude (km)	Observer's Comments
23	June 04	14:01	15:16	24.3	no comment
24	June 04	16:50	18:15	25.5	no comment
25	June 04	22:51	00:10	24.9	Perfect flight
26	June 05	05:05	06:16	21.5	1 balloon broke. 3/4 full. Launch good
27	June 05	07:55	09:06	23.7	no comment
28	June 05	10:51	12:15	24.7	no comment
29	June 05	13:50	15:15	25.3	no comment
30	June 05	16:47	18:02	24.8	no comment
31	June 05	22:55	00:12	24.8	Winds below 700mb questionable. Signal strength was low and tracking was to SW but balloon was to SSE.
32	June 06	05:02	06:17	21.5	Drizzle during second half of flight. Turned to light rain at 06:05.
33	June 06	07:58	09:15	20.7	no comment
34	June 06	10:51	12:06	24.5	no comment
35	June 06	13:46	15:03	25.3	Some data lost in stratosphere
36	June 06	16:54	18:14	22.2	Debris 10% Sc,Cu 50%
37	June 06	23:03	23:30	7.7	Could not auto track. No wind data. Flight terminated early.
38	June 07	04:59	06:44	25.2	Good launch. Auto track acquired after about 100m height. Balloon burst at about 13 mb.
39	June 07	08:06	09:28	26.5	Clear sky
40	June 07	10:56	12:17	24.5	Some data lost below about 100m height. Cu 5%, Cist 10%.
41	June 07	16:49	17:48	19.1	30% Cu, watched balloon go through cloud edge
42	June 07	22:51	00:19	22.0	Fractional cloudiness was small at launch but balloon went right up through a low cloud. Some interesting behavior of T & RH at cloud top-perhaps due to sensor wetting.
43	June 08	04:56	06:42	15.0	This sounding was made with a low ascent rate (2.1 m/s) in lower half. An excellent sounding with much detail.
44	June 08	08:30	09:50	26.0	Delayed launch due to generator maintenance. 30% Cu

Sounding Number	Date	Start Time (UTC)	End Time (UTC)	Maximum Altitude (km)	Observer's Comments
45	June 08	10:57	12:14	24.1	30% Cu here, stratus to north
46	June 08	13:59	15:44	25.3	Thin Sc
47	June 08	16:50	18:12	20.0	Sc and Cu
48	June 08	22:48	00:19	19.5	Light rain at 12:31 winds around 140 mb and above have low elevation.
49	June 08	01:44	04:04	24.9	Winds above 100 mb look questionable due to low elevation. Burst at 19mb.
50	June 09	04:53	05:21	5.8	Did not auto track at launch but was acquired in first 200m. Sonde had very low signal. Lost it at 500m.
51	June 09	08:05	09:17	19.3	Bad humidity sonde, not aspirated
52	June 09	11:07	12:13	18.6	no comment
53	June 09	14:07	15:18	22.5	no comment
54	June 09	17:03	18:08	20.8	1st sonde bad: no signal
55	June 09	22:52	23:31	11.7	Radar has 15km region over us. No drizzle at launch; very light when sonde at 650 mb. Good sounding to 319 mb, but suddenly quit there.
56	June 09	01:52	03:21	24.0	Excellent flight. Burst at about 30mb.
57	June 10	04:55	05:47	14.5	Good sounding. Sonde quit at about 150mb.
58	June 10	07:54	09:14	25.1	Surface levels lost. Opr error
59	June 10	13:03	14:28	23.5	no comment
60	June 10	16:55	18:16	26.2	no comment
61	June 10	19:42	21:28	25.5	Scattered Cu, some Cist. Lost first 300m.
62	June 10	22:47	00:15	24.2	Dark, light shower
63	June 10	02:01	03:57	28.9	Cu. Burst at about 15 mb
64	June 11	04:49	06:13	21.3	Mostly clear
65	June 11	08:09	09:18	17.5	Ceiling 8:14:03 888 mb Cu hum
66	June 11	11:03	12:19	22.7	Cu hum
67	June 11	14:03	15:19	18.9	Cu hum

Sounding Number	Date	Start Time (UTC)	End Time (UTC)	Maximum Altitude (km)	Observer's Comments
68	June 11	16:53	18:17	21.7	Sc
69	June 11	20:05	21:17	9.9	Cu, Ci, St. Lost signal for awhile, twice.
70	June 11	22:46	00:05	20.8	Drizzle
71	June 12	01:50	03:36	24.5	Drizzle
72	June 12	04:45	06:17	23.0	Cloudy
73	June 12	08:07	09:18	18.2	Cloudy - adjusted pressure
74	June 12	10:51	12:19	26.3	Cloudy
75	June 12	13:51	15:19	26.1	Cloudy - rain
76	June 12	16:52	18:17	20.8	Cloudy
77	June 12	20:06	21:23	17.3	Sc
78	June 12	22:49	00:15	21.0	Drizzle
79	June 13	01:53	03:14	11.4	Drizzle. Humidity not good
80	June 13	05:38	06:39	17.0	Clear Sc Software problem-delayed launch.
81	June 13	07:50	09:28	25.3	Good sounding to 30mb
82	June 13	10:47	12:19	23.4	Good sounding
83	June 13	14:01	15:32	24.7	Good sounding to 30mb
84	June 13	16:52	18:20	22.0	Good sounding to 41mb
85	June 13	19:58	21:29	23.5	Sc, RH suspect in upper troposphere.
86	June 13	22:59	00:17	21.0	Sc, dramatic RH drop in above cloud, RH suspect again - very low in mid troposphere.
87	June 14	01:52	03:25	27.7	Sc BINOVC similar to last sounding.
88	June 14	05:42	06:17	7.9	Sc BINOVC; RH<95% in cloud; ceilometer cloud base=1100m, ceilometer cloud top=1400m.
89	June 14	07:54	09:25	26.4	Good sounding up to 150mb. Signal weak above this. Burst at 32mb.
90	June 14	10:52	12:10	16.4	Hygristor shield fell off at launch. Radiation error in humidity? Signal lost at 100mb.
91	June 14	13:53	15:37	25.3	Good sounding to 12.4mb
92	June 14	16:47	18:20	22.4	Did not auto track at launch but acquired in about 30s.
93	June 14	20:09	22:00	25.3	1st sonde stopped transmitting at launch. 2nd launch accomplished to 16mb.
94	June 14 June 15	23:00	23:59	16.6	Cu. RH no good above 320mb? Cu hum. Balloon burst and sonde fell at 534 mb.

Sounding Number	Date	Start Time (UTC)	End Time (UTC)	Maximum Altitude (km)	Observer's Comments
	June 15				Cu hum. RH no good above 350 mb?
	June 15				Cu hum. Good winds to >50 mb. RH no good above 320 mb?
95	June 15	07:57	09:13	15.3	Cu and St
96	June 15	10:50	12:19	25.4	Cu, haze
	June 15				Broken Sc, haze
97	June 15	16:56	18:19	15.8	Cu, some
98	June 15	19:49	21:41	25.3	Cu; balloon burst at 12.8 mb
	June 15				Cu to Sc. Balloon sank at 764 mb
99	June 15	23:32	00:19	17.6	Sc. Pressure bad <310 mb
100	June 16	01:58	03:18	21.7	Sc. lost at first, recovered by 1 min
101	June 16	04:54	06:24	21.9	Cu fra
102	June 16	07:58	09:34	25.4	Broken Sc. Did not auto track at launch. Lost lowest few hundred meters
103	June 16	10:55	12:19	17.2	Few ragged looking Cu
104	June 16	13:47	15:49	30.0	Scattered Cu and haze
105	June 16	16:56	18:14	15.4	Cu, haze
106	June 16	20:17	21:29	20.9	Cu fra, hum
107	June 16	22:52	00:18	23.2	Overcast, occasional drizzle
108	June 17	01:56	03:08	21.0	Overcast
109	June 17	04:52	06:18	24.1	Overcast
110	June 17	08:04	09:25	18.1	Overcast stratus; drizzle
111	June 17	10:53	12:14	18.7	Overcast stratus
112	June 17	13:54	15:29	23.7	Overcast
113	June 17	16:59	18:18	13.0	Complete overcast of stratus
114	June 17	19:59	21:11	20.7	Intermittent sonde. Partly cloudy
115	June 17	22:51	00:15	21.2	Mostly clear
116	June 18	01:49	03:13	22.7	Cloudy
117	June 18	04:53	06:11	22.9	Cloudy
118	June 18	07:53	09:46	28.0	St
119	June 18	10:55	12:41	27.9	St
120	June 18	13:54	15:28	22.1	Cloudy
121	June 18	16:51	18:17	17.4	Scattered Cu, mostly clear

Sounding Number	Date	Start Time (UTC)	End Time (UTC)	Maximum Altitude (km)	Observer's Comments
122	June 18	20:01	21:18	21.0	Mostly clear. Lost at 90 mb, regained at 69 mb.
123	June 18	22:49	00:15	23.4	Cloudy
124	June 19	01:54	03:15	23.6	Thin clouds
125	June 19	04:53	05:54	16.3	Cloudy. Lost then reacquired sonde at launch. Sonde lost due to interference at 1671 MHz.
126	June 19	07:53	10:00	25.9	Overcast 5000 ft. Some low cloud at 3000 ft. Sonde reached 11.1 mb.
127	June 19	10:54	12:21	14.8	Scattered 2/10 5000 ft, 1/10 1500 ft.
128	June 19	13:57	15:49	25.3	50% cloud cover. Good sounding to 11.9 mb.
	June 19				10% cloud cover. Balloon burst (or leak) at 890 mb. Launched 2nd balloon.
129	June 19	17:07	18:20	16.6	10% cloud cover
	June 19				Bad sonde or something
	June 19				Bad sonde
130	June 19	20:48	22:12	22.9	Launch occurred at 20:50 GMT. Lots of trouble with other two.
131	June 19	22:53	00:11	21.9	no comment
132	June 20	01:57	03:03	17.2	no comment
133	June 20	04:54	05:55	17.4	no comment
134	June 20	07:41	09:54	31.4	Cu with St above. Reached 10.2 mb.
135	June 20	10:44	12:17	22.7	Ci and Cu
136	June 20	13:45	15:44	27.0	Broken St
137	June 20	16:46	18:19	22.6	Cu, Ci
138	June 20	19:59	21:21	18.6	Cu 5%, Haze
139	June 20	22:57	23:52	12.5	Balloon burst at 190 mb
140	June 21	02:03	04:14	25.4	no comment
141	June 21	04:58	06:18	20.8	Stratus 4200-4700 ft. Terminated at 50 mb.
142	June 21	07:51	09:10	22.7	Stratus; drizzle at 8:23Z
143	June 21	10:48	12:16	13.4	Stratus
144	June 21	13:52	14:51	13.4	Cu, broken, high stratus (next to last brown balloon).
145	June 21	16:56	18:20	14.9	Cu
146	June 21	19:45	21:16	21.8	Broken Cu. Light drizzle on launch
147	June 21	22:54	00:14	22.3	Drizzle
148	June 22	01:54	03:42	22.6	Noisy hygistor
149	June 22	04:58	06:18	20.8	Stopped at 50 mb. Overcast, light drizzle.

Sounding Number	Date	Start Time (UTC)	End Time (UTC)	Maximum Altitude (km)	Observer's Comments
150	June 22	07:39	09:24	25.2	Cu with St above
151	June 22	10:45	12:14	25.4	Cu with St above
152	June 22	13:44	15:20	23.9	Cu with St above
153	June 22	16:41	18:32	23.6	Thin Sc, some thicker blobs
154	June 22	20:01	21:56	23.8	Cu, St
155	June 22	22:53	00:16	19.2	no comment
156	June 23	01:51	03:21	22.0	no comment
157	June 23	04:52	06:02	21.1	no comment
158	June 23	07:49	08:55	20.1	Cu below St. Lowest 50 mb lost
159	June 23	10:47	12:00	21.9	Light rain. Cu below St.
160	June 23	13:47	15:38	24.5	Broken Sc
161	June 23	16:51	18:08	22.4	Ci and some Cu
162	June 23	19:56	21:03	19.8	Cu
163	June 23	22:50	00:01	21.2	no comment
164	June 24	01:50	02:38	13.8	Widely scattered Cu. Lost signal at 139 mb.
165	June 24	05:04	06:16	22.2	Thin stratus
166	June 24	07:51	09:04	23.0	Cloud base at 857 m. Data gap near 200 mb.
167	June 24	10:44	11:48	21.7	Cu below St
168	June 24	13:54	15:16	22.5	Cu below St. Some holes
169	June 24	16:46	18:08	23.2	Cu penetrating into a broken layer cloud at 2000 ft. Bad pressure sensor.
170	June 24	19:57	21:16	15.2	Few scattered Cu 5%
171	June 24	22:58	00:15	18.8	Clear
172	June 25	01:44	03:23	22.0	Clear
173	June 25	04:58	06:15	22.2	Thin stratus
174	June 25	07:49	09:07	21.7	Sonde intermittent above 200 mb
175	June 25	10:51	12:03	22.6	no comment
176	June 25	13:51	14:53	21.5	no comment
177	June 25	16:47	18:15	24.1	no comment
178	June 25	19:44	21:32	25.1	Mostly clear
179	June 25	22:46	00:20	22.5	Clear
180	June 26	01:48	03:32	24.6	Clear. Can see stars. A little foggy at surface. RH decreased with height.
181	June 26	04:37	06:07	23.4	Clear. May be thin surface inversion. RH decreased with height initially again.
182	June 26	07:49	09:04	22.3	Lost tracking in lowest 50 mb
183	June 26	10:55	12:07	22.2	no comment
184	June 26	13:51	15:08	23.6	Did not autotrack at launch but regained in 30 s.
185	June 26	16:48	17:49	21.6	Lost track in lowest 50 mb
186	June 26	19:51	20:59	22.5	Almost completely clear
187	June 26	22:51	00:48	25.9	Clear

Sounding Number	Date	Start Time (UTC)	End Time (UTC)	Maximum Altitude (km)	Observer's Comments
188	June 27	01:59	03:17	22.8	Did not autotrack at launch but regained at about 900 mb. AFC failed between 500 mb and 425 mb.
189	June 27	04:49	06:04	22.0	Less than 10% cloud cover
190	June 27	07:50	09:02	21.1	Severe clear
191	June 27	10:49	11:54	21.1	no comment
192	June 27	13:51	14:45	17.6	Ci. Mostly clear. Lost at 83 mb. Vapor=3.69.
193	June 27	16:40	17:21	11.4	Hygristor cover fell off at launch. 4 balloons!
194	June 27	20:08	21:28	21.5	Clear except St on N horizon. Lost hygristor cover.
195	June 27	22:59	00:19	17.8	Very clear
196	June 27	01:48	03:20	22.5	No visible cloud
197	June 28	04:50	06:13	21.4	No cloud
198	June 28	07:46	09:12	23.3	Did not autotrack at launch, regained in about 10s.
199	June 28	10:45	12:04	21.2	Cumulus scattered. Sonde entered cloud soon after launch (about 300 mb).
200	June 28	13:48	15:18	23.3	Scattered Cu
201	June 28	16:47	18:05	22.0	Cloud overhead with breaks to the North.
202	June 28	20:14	21:54	22.6	Broken St
203	June 28	22:53	00:25	21.0	Cloudy; RT failed to track but we regained. Did not lose signal. Winds garbage, below 750 mb.

APPENDIX 2: INSTRUCTIONS FOR DISPLAYING CAMPBELL STATION DATA IN SPECTRA CALC

1. START SPECTRA CALC
CD\SC
SC

2. LOAD FILE
F2
ARITHMETIC
DEPROGRAM
STATION1
ENTER FILENAME:

USE ARROWS TO LOCATE DATA ON JULIAN DAY SCALE
USE PAGE UP/PAGE DN TO DISPLAY DIFFERENT VARIABLES
USE ALT-N TO DELETE UNWANTED VARIABLES

3. SELECT TEMPLATE
F2
ENVIRONMENT
TEMPLATE
RETRIEVE

TEMPLATE NAME	VARIABLE NAME
ASTEMP	TEMP
ASRELH	RELHUM
ASSOIR	SWTOT
ASIRIR	IR

USE ARROWS TO LOCATE DATA ON ABCISSA SCALE

3. PLOT GRAPH
F2
PLOT
GRAPHICS PRINTER

**APPENDIX 3: PRT 6 CALIBRATION FROM INTERFEROMETER DATA
(USING SPECTRA CALC)**

1. RECORD TIMES FROM ORIGINAL INTERFEROGRAM FILE
2. START SPECTRA CALC
LOAD SPECTRUM FILE
F2
FILE
RETRIEVE - SPECTRUM FILE
FILE NAME .SPC
F4 [TO SEE ALL OF SPECTRA]

LOAD TEMPLATE WHICH CLIPS SPECTRUM TO PRT6 BANDPASS
F2
ENVIRONMENT
TEMPLATE
RETRIEVE
"PRT6CAL"
RETURN

PERFORM INTEGRATION ACROSS PRT6 BANDPASS
F2
ARITHMETIC
OTHER
FUNCTION
INTEGRATION
SINGLE PEAK
[NO BASELINE CORRECTION]
ENTER
MANUALLY RECORD INTEGRATED RADIANCE [AREA]
W M-2 STER-1
EXIT
ALT N TO CLEAR SPECTRUM
3. LOCATE PRT6 OUTPUT VOLTAGE FOR INTERFEROGRAM
COLLECTION TIMES
4. PLOT PRT6 VALUES VS. AREA INTEGRATED INTERFEROMETER
RADIANCES

APPENDIX 4: CAMPBELL PRT6 DATA UPLOAD

1. ENTER CAMPBELL SUBDIRECTORY ON DRIVE D:
 D:\CAMPBELL

2. CHECK FOR PREVIOUS DATA FILE "PRT6.DAT"
 - A. ORDINARILY IT SHOULD NOT BE PRESENT; IF IT IS NOT,
 PROCEED TO STEP 3.
 - B. IF THE FILE IS PRESENT PLACE IT IN THE ARCHIVE
 - i. TYPE: COPY PRT6.DAT mmddPff.dat
 where P is a constant
 ff is a sequential integer starting with 1 each UT day and
 incrementing by 1 each subsequent data upload
 - ii. After verifying successful copy of file by comparing file sizes of
 PRT6.DAT and mmddPff.dat, erase PRT6.DAT

 TYPE: DEL PRT6.DAT

3. UPLOAD DATA FROM CAMPBELL
 TYPE: TELCOM PRT6 /C

4. AFTER LISTING OF HEX FILE INDICES, COPY DATA FILE TO ARCHIVE
 TYPE: COPY PRT6.DAT mmddPff.dat (see B,i. above for format)
 - i. TYPE: COPY PRT6.DAT mmddPff.dat
 where P is a constant
 ff is a sequential integer starting with 1 each UT
 day and incrementing by 1 each subsequent data
 upload
 - ii. After verifying successful copy of file by comparing file sizes of
 PRT6.DAT and mmddPff.dat, erase PRT6.DAT

 TYPE: DEL PRT6.DAT

CAMPBELL PRT6 PROGRAM DOWNLOAD FROM PC

1. TYPE: D:\CAMPBELL
2. TYPE: TERM PRT6
3. SELECT "D" FOR DOWNLOAD
4. ANSWER PROMPT: NAME OF PROGRAM TO DOWNLOAD? BY TYPING PRT6
5. AT THE PRT6.DLD LABEL PROMPT, HIT "RETURN"
6. AFTER DOWNLOAD IS COMPLETED YOU WILL BE PROMPTED TO EXIT WITH CNTRL-.
7. DOWNLOAD PC CLOCK TIME TO CAMPBELL, SELECT "K"
8. QUIT, SELECT "Q"

APPENDIX 5: INTERFEROMETER OPERATION INSTRUCTIONS

1. TURN ON POWER
INTERFEROMETER
MOTOR POWER SUPPLY
CAMPBELL
2. SET UP MOTOR POSITION
C: DRIVE CD MOTOR
RESETC [SCANS FOR ZERO POSITION]
CD\SC [GO TO SPECTRA CALC SUBDIRECTORY]
MIRROR 243 [COLD BB POSITION]
SC [SPECTRA CALC]
F2
COLLECT
ENTER BOGUS NAME: TEST
[SHOULD DISPLAY NOISY INTERFEROGRAM]
GO
3. REMOVE CAP ON INTERIOR LENS
REMOVE CAP ON EXTERIOR LENS
REMOVE CAP ON AMBIENT BLACK BODY
4. REMOVE ROOF CAP
5. OPEN MAIN CO₂ VALVE - P MUST BE > 2000 PSI
SLOWLY OPEN GRAY VALVE TO 100-200 PSI TO PURGE LINE
OPEN BLACK HANDLED LINE VALVE [PURGE FOR AT LEAST FIVE
MINUTES]
6. FILL BLACK BODY DEWAR AND INSTALL WITH STYROFOAM COLLAR
& AL CYLINDER
8. CHECK FOR LASER POSITION ON MIRROR
9. TURN GRAY KNOB ON CO₂ TANK TO PSI > 1700-2000 PSI TO COOL
DETECTOR.
10. OBSERVE LESS NOISE ON INTERFEROGRAM AS DETECTOR COOLS.
11. SET UP CAMPBELL FOR DOWNLOAD
D:\CAMPBELL
TERM BOM21
D [DOWNLOAD]
NAME OF PROGRAM ... "BOM21"

CNTRL- [TO EXIT BACK TO MENU]

K [PC TIME TO DATA LOGGER]

M [MONITOR INPUT LOCATION]

DISPLAYS

1 REF TEMP DISK > AMBIENT AIR TEMP (4)

2 Cu cavity Black Body

3 Cu cavity Black Body

4 Ambient air temp

CNTRL-

Q

12. MANUAL SAMPLE RETRIEVAL

TELCOM BOM21 /C [WRITES IN BOM21.DAT]

DISPLAY IN PC WRITE

DELETE BOM21.DAT

13. NEXT GO BACK TO SPECTRA CALC

CD\SC

SC

F2

COLLECT

ALIGN

F4 [AUTOSCALE]

WHEN INTERFEROGRAM CONVERGES - READY TO COLLECT SPECTRUM

Esc [One step before align]

Check: Type

Scan

Align

Edit if necessary

14. START DATA/INTERFEROGRAM COLLECTION

F2

ARITHMETIC

DOPROGRAM

"COLBOM"

ENTER # OF CYCLES

BASE FILE NAME: MMDDi

ENTER BEGINNING FILE NO. [Same as last # on previous spectra with same file name: mmddi

ENTER NO OF SCANS: (20)

NO DISPLAY DURING INTERFEROGRAM DATA COLLECTION

15. AFTER DISPLAY RETURNS

HIT ESC

F2

FILE

RETRIEVE

F4 [TO SEE ALL]

MMDDIXX LN₂ BLACK BODY WHERE XX= 01 + N*3

MMDDIXX AMB. BLACK BODY XX= 02 + N*3

MMDDIXX ATMOS. SPECTRA XX= 03 + N*3

QUIT TO LEAVE SC

16. D:\CAMPBELL [GO TO CAMPBELL SUBDIRECTORY IN D:]
LABEL FILES TO KEEP THEM STRAIGHT

COPY BOM21.DAT JU04BXX.DAT

XX IS THE NO. OF LAST INTERFEROGRAM RECORDED

DEL BOM21.DAT

INTERFEROMETER SYSTEM SHUTDOWN

TO SHUT DOWN THE SYSTEM

- 1. REMOVE MIRROR [USE ALLEN WRENCH] SET ASIDE**
- 2. PUT COVER ON EXTERNAL INTERFEROMETER LENS**
- 3. REMOVE LNO₂ BLACK BODY DEWAR**
- 4. POUR LN₂ INTO SMALL DEWAR AND THEN TRANSFER TO LARGE DEWAR**
- 5. TURN OFF MAIN CO₂ VALVE**
- 6. COVER INTERNAL LENS**
- 7. COVER AMBIENT BLACK BODY**
- 8. TURN OFF MAIN CO₂ VALVE**
- 9. TURN OFF INSTRUMENTS**
CAMPBELL
MOTOR POWER SUPPLY
INTERFEROMETER

**APPENDIX 6: INTERFEROMETER SPECTRA REDUCTION
(Convert Interferograms to Spectra)**

1. MOVE SET OF THREE INTERFEROGRAM FILES AND BOMEM.DAT [CAMPBELL BLACK BODY FILE {mmddb03.dat}] TO D:\SC
2. EDIT TEMPERATURE DATA FROM mmddb03.dat file [USE PC WRITE]
NOTE: NO BEFORE .DAT WILL ALWAYS BE A MULTIPLE OF 3
 - A. REMOVE EOF INDICATOR AFTER LAST RECORD
 - B. MOVE SET OF TEMPERATURE TO INTERMEDIATE FILE
[12 DATA LINES FOR EACH SPECTRUM - 4/INTERFEROGRAM]
INTERMEDIATE FILE NAME: mmddb03a.dat
 - C. REPEAT FOR ADDITIONAL SPECTRA
USE FILE NOTATION :mmddb03b.dat, etc.
3. READ AND AVERAGE BLACK BODY TEMPERATURE FILES
 - A. RUN RECAP
 - B. PROMPT FOR INPUT FILE: mmddb03a.dat
 - C. PROMPT FOR OUTPUT FILE: mmddb03a.out
 - D. REPEAT for additional spectra
4. COPY INTERFEROGRAM FILES INTO APPROPRIATE DUMMY VARIABLE NAMES
Copy mmddi01.spc bbcold.spc
Copy mmddi02.spc bbhot.spc
Copy mmddi03.spc atmos.spc
5. If Windows has not been booted, do it now.
6. PERFORM CALIBRATION AND PRODUCE SPECTRUM
D:\SC
SC
F2
ARITHMETIC
DOPROGRAM
SPSAVE
mmddb03a.out

Esc
Esc [Returns to main menu]

Files as displayed are overlaid - put into page mode

F2
 Environ
 Multiple Spectra
 Paged

7. Save Spectrum

F2
File
Save
 mmdds03

8. To compare with other files

F2
File
Retrieve
 [Use alt<N> to delete unwanted files from page buffer

9. To overlay

A. Remove unwanted spectra [Alt<N>
B. F2
 Environment
 Multiple Spectra
 Overlaid

APPENDIX 7: CEILOMETER OPERATIONS PROCEDURES

1. Ensure ceilometer circuit breaker at the generator is turned on.
2. On ceilometer PC, press "Caps Lock" key. Go to the C:\CLOUDS directory.
3. Type "procomm." In Procomm, do CNTRL-C. When prompted for password, type COD0 (must be capital letters).
4. Type ":". To set time, type in seconds - space - minutes - space, etc. until you are prompted to turn the oscillator on. Type 0 - ENTER. To start the new time press ENTER.
5. Type E - ENTER - CNTRL-A - O - P - ENTER.
6. Exit procomm by ALT-X.
7. From DOS (C:\CLOUDS), type "HIST."
8. After the histogram software has started, press F8 to record data. When asked for filename, enter YYMMDDHH.RAW, where YY=year, MM=month, DD=day, HH=hour (GMT).

APPENDIX 8: FUNCTIONS OF CONTROL KEYS FOR THE CEILOMETER HISTOGRAM PROGRAM

The histogram program is controlled by the use of the programmable function "F" keys (F1 - F10) and the "Alt" and "Shift" keys combined with other keys. The function of some of the "F" keys changes depending on the present mode of operation.

GENERAL PROGRAM CONTROL

"F" KEYS	PRIMARY FUNCTION	SECONDARY FUNCTION
F1	Toggle Auto/Manual Clear	
F2	Clear Graphics Screen (Manual)	
F3	Toggle Klett processing ON/OFF	Increment playback frame
F4	Decrement playback frame	
F5	Toggle Auto/Manual playback mode	Copy Transfer
F6	Playback next frame	
F7	Toggle Playback mode	
F8	Toggle Record mode	Toggle Klett processing ON/OFF
F9	Toggle Copy mode	
F10	Exit program	

GRAPHICS SCREEN GRID CONTROL

Home - Controls the left end of the GRID
End - Controls the right end of the GRID
PgUp - Controls the top of the GRID
PgDn - Controls the bottom of the GRID

Alt - Decrements the selected parameter
Shift - Decrements the selected parameter

Alt-Home - Decrements the right side of the GRID. This brings the far range closer in.
Alt-End - Decrements the left side of the GRID. This brings the near range closer in.
Alt-PgUp - Decrements the top of the GRID. This reduces the positive amplitude range.
Alt-PgDn - Decrements the bottom of the GRID. This the increases negative amplitude range.

Shift-Home - Increments the right side of the GRID. This pushes the far range farther out.

Shift-End - Increments the left side of the GRID. This pushes the near range farther out.

Shift-PgUp - Increments the top of the GRID. This increases the positive amplitude range.

Shift-PgDn - Increments the bottom of the GRID. This reduces the negative amplitude range.

GRID PARAMETER LIMITS	LOWER LIMIT	UPPER LIMIT	DEFAULT
left side (near range)	-250	25000	0
right side (far range)	250	25500	25500
top (positive amplitude)	-190	2550	1500
bottom (negative amplitude)	-2550	-110	-200

The range axis (X axis) of the histogram is in units of feet.

The amplitude axis (Y axis) of the histogram is in units of signal return counts.

Note: The amplitude is derived in part by:

LIDAR profile => signal returns - noise returns

A natural side effect of this is that the resultant signal return counts can go negative. This IS meaningful.

APPENDIX 9: WIND PROFILER PARAMETERS

RADAR PARAMETERS

CONTACT: Dave

DATE OF CHANGE: 27 MAY 92 L

		MODE 1		MODE 2		MODE 3		MODE 4		MODE 5		MODE 6	
PARAMETER	UNIT	NORM	NEW	NORM	NEW	NORM	NEW	NORM	NEW	NORM	NEW	NORM	NEW
ANT_DIR	CODE	0		0		1		1		2		3	2
ARA	O/I	1		1		1		1		1		1	0
CCP_GAIN	N	6		6		6		6		6		6	
CODE	CODE	0		0		0		0		0		0	
CON_DELAY	m/s	2.00e0		2.00e0		2.00e0		2.00e0		2.00e0		2.00e0	
DELAY	1/6 μs	300		32		300		32		300		32	35
DODC	O/I	1		1		1		1		1		1	
FILTER	CODE	1		0		1		0		1		0	
GCNUM	N	3		2		3		2		3		2	21
POW_FACTOR	REAL	4.67e-4		4.67e-4		4.67e-4		4.67e-4		4.67e-4		4.67e-4	
PRP	0.1 μs	2400		1000		2400		1000		2400		1000	1045
PW_BAUD	1/6 μs	40		10		40		10		40		10	
RX_DELAY	0.01 μs	397		208		397		208		397		208	
RX_GAIN	N	255		255		255		255		255		255	
SAMPLE_MIN	N	4		4		4		4		4		4	
SPACE	1/6 μs	10		10		10		10		10		10	
SPAN	N	63		63		63		63		63		63	128
SPECTRA	N	46		35		46		35		26		28	
SSTDODC	O/I	1		1		1		1		1		1	
TDA	N	24		64		24		64		24		80	60
WINDOW	O/I	1		1		1		1		1		1	
DOPOWCOR	O/I	0		0		0		0		0		0	
COMMON PARMS		UNIT	NORM	NEW									
BLANK_TX	1/2 μs	15		NOTES: $f_{off5} = 956.9$ $C_{off5} = 354.75$									
CONSENSUS_SET	N	12											
COOLDOWN	S	0		$T = \left[\frac{C_{off5} - N_{app}}{20.047} \right]^2 - 273.15 \text{ } ^\circ\text{C}$									
FREEDLAY	10 ms	50											
NUMGATES	N	36											
NUMMODES	N	10		initial setup									
TR_TX	1/2 μs	10											
TX_BLANK	1/6 μs	10											
TX_DUTY	0.1%	50											
TX_TR	1/6 μs	8											

27 MAY 92

PARAMETER	UNIT	MODE 7		MODE 8		MODE 9		MODE 10		MODE 11		MODE 12	
		NORM	NEW										
ANT_DIR	CODE	4		4		5		5					
ARA	O/I	1		1		1		1					
CCP_GAIN	N	6		6		6		6					
CODE	CODE	0		0		0		0					
CON_DELTAV	M/S	2000		2000		2000		2000					
DELAY	% US	300		32		300		32					
DODC	C/I	1		1		1		1					
FILTER	CODE	1		0		1		0					
GCNUM	N	3		2		3		2					
POW_FACTOR	REAL	4.67e-9		4.67e-9		4.67e-9		4.67e-9					
PRP	0.1 US	2400		1000		2400		1000					
PW_BAUD	% US	40		10		40		10					
RX_DELAY	0.1 US	397		208		397		208					
RX_GAIN	N	255		255		255		255					
SAMPLE_MIN	N	4		4		4		4					
SPACE	% US	10		10		10		10					
SPAN	N	63		63		63		63					
SPECTRA	N	46		35		46		35					
SSTDODC	O/I	1		1		1		1					
TDA	N	24		64		24		64					
WINDOW	O/I	1		1		1		1					
DOPOWCOR	O/I	0		0		0		0					

RADAR PARAMETERS

6/1/92

CONTACT: Dave

DATE OF CHANGE: 805 ZULU

PARAMETER	UNIT	MODE 1		MODE 2		MODE 3		MODE 4		MODE 5		MODE 6	
		NORM	NEW										
ANT_DIR	CODE	0		0		1		1		2		3	2
ARA	O/I	1		1		1		1		1		1	0
CCP_GAIN	N	6		6		6		6		6		6	
CODE	CODE	0		0		0		0		0		0	
CON_DELAY	m/s	2.00e0											
DELAY	1/6 μs	300		32		300		32		300		32	35
DODC	O/I	1		1		1		1		1		1	
FILTER	CODE	1		0		1		0		1		0	
GCNUM	N	3		2		3		2		3		2	21
POW_FACTOR	REAL	4.67e-4											
PRP	0.1 μs	2400		1000		2400		1000		2400		1000	1045
PW_BAUD	1/6 μs	40		10		40		10		40		10	
RX_DELAY	0.01 μs	397		208		397		208		397		208	
RX_GAIN	N	255		255		255		255		255		255	
SAMPLE_MIN	N	4		4		4		4		4		4	
SPACE	1/6 μs	10		10		10		10		10		10	
SPAN	N	63		63		63		63		63		63	128
SPECTRA	N	46		35		46		35		26		28	
SSTDODC	O/I	1		1		1		1		1		1	
TDA	N	24		64		24		64		24		80	60
WINDOW	O/I	1		1		1		1		1		1	
DOPOWCOR	O/I	0		0		0		0		0		0	

COMMON PARMS	UNIT	NORM	NEW
--------------	------	------	-----

BLANK_TX	1/2 μs	15	
CONSENSUS_SET	N	12	
COOLDOWN	S	0	
FREEDLAY	10 ms	50	
NUMGATES	N	36	
NUMMODES	N	10	
TR_TX	1/2 μs	10	
TX_BLANK	1/6 μs	10	
TX_DUTY	0.1%	50	
TX_TR	1/6 μs	8	

NOTES:

$f_{offs} = 956.9$ $g_{offs} = 354.75$

$$T = \left[\frac{V_{offs} - V_{app}}{20.247} \right]^2 - 273.15 \text{ } ^\circ\text{C}$$

changed mode 9 to Low vert

6/1/92

805Z

PARAMETER	UNIT	MODE 7		MODE 8		MODE 9		MODE 10		MODE 11		MODE 12	
		NORM	NEW	NORM	NEW	NORM	NEW	NORM	NEW	NORM	NEW	NORM	NEW
ANT_DIR	CODE	4		4		5	3	5					
ARA	O/I	1		1		1		1					
CCP_GAIN	N	6		6		6		6					
CODE	CODE	0		0		0		0					
CON_DELTAV	M/S	2000		2000		2000		2000					
DELAY	%US	300		32		300	32	32					
DODC	O/I	1		1		1		1					
FILTER	CODE	1		0		1	0	0					
GCNUM	N	3		2		3	2	2					
POW_FACTOR	REAL	4.67e-4		4.07e-4		4.67e-4		4.67e-4					
PRP	0.1US	2400		1000		2400	1000	1000					
PW_BAUD	%US	40		10		40	10	10					
RX_DELAY	0.1US	397		208		397	208	208					
RX_GAIN	N	255		255		255		255					
SAMPLE_MIN	N	4		4		4		4					
SPACE	%US	10		10		10		10					
SPAN	N	63		3		63		63					
SPECTRA	N	46		5		46	28	35					
SSTDODC	O/I	1		1		1		1					
TDA	N	24		64		24	80	64					
WINDOW	O/I	1		1		1		1					
DOPOWCR	O/I	0		0		0		0					

RADAR PARAMETERS

6/2/92
 CONTACT: Dave DATE OF CHANGE: 10292

PARAMETER	UNIT	MODE 1		MODE 2		MODE 3		MODE 4		MODE 5		MODE 6	
		NORM	NEW										
ANT_DIR	CODE	0		0		1		1		2		3	2
ARA	O/I	1		1		1		1		1		1	0
CCP_GAIN	N	6		6		6		6		6		6	
CODE	CODE	0		0		0		0		0		0	
CON_DELTA	m/s	2.00e0											
DELAY	1/6 μs	300		32		300		32		300		32	35
DODC	O/I	1		1		1		1		1		1	
FILTER	CODE	1		0		1		0		1		0	
GCNUM	N	3		2		3		2		3		2	21
POW_FACTOR	REAL	4.67e-4											
PRP	0.1 μs	2400		1000		2400		1000		2400		1000	1045
PW_BAUD	1/6 μs	40		10		40		10		40		10	
RX_DELAY	0.01 μs	397		208		397		208		397		208	
RX_GAIN	N	255		255		255		255		255		255	
SAMPLE_MIN	N	4		4		4		4		4		4	
SPACE	1/6 μs	10		10		10		10		10		10	
SPAN	N	63		63		63		63		63		63	127
SPECTRA	N	46		35		46		35		26		28	40
SSTDODC	O/I	1		1		1		1		1		1	
TDA	N	24		64		24		64		24		80	60
WINDOW	O/I	1		1		1		1		1		1	
DOPOWCOR	O/I	0		0		0		0		0		0	

COMMON PARMS	UNIT	NORM	NEW
--------------	------	------	-----

COMMON PARMS	UNIT	NORM	NEW	NOTES
BLANK_TX	1/2 μs	15		changed mode 6 SPECTRA TO 40
CONSENSUS_SET	N	12		
COOLDOWN	S	0		
FREEDLAY	10 ms	50		
NUMGATES	N	36		
NUMMODES	N	10		
TR_TX	1/2 μs	10		
TX_BLANK	1/6 μs	10		
TX_DUTY	0.1%	50		
TX_TR	1/6 μs	8		

6/2/92

1029Z

PARAMETER	UNIT	MODE 7		MODE 8		MODE 9		MODE 10		MODE 11		MODE 12	
		NORM	NEW	NORM	NEW	NORM	NEW	NORM	NEW	NORM	NEW	NORM	NEW
ANT_DIR	CODE	4		4		5	3	5					
ARA	O/I	1		1		1		1					
CCP_GAIN	N	6		6		6		6					
CODE	CODE	0		0		0		0					
CON_DELTAV	M/S	2000		2000		2000		2000					
DELAY	%US	300		32		300	32	32					
DODC	O/I	1		1		1		1					
FILTER	CODE	1		0		1	0	0					
GCNUM	N	3		2		3	2	2					
POW_FACTOR	REAL	4.67e-9		4.67e-9		4.67e-9		4.67e-9					
PRP	0.1US	2400		1000		2400	1000	1000					
PW_BAUD	%US	40		10		40	1	10					
RX_DELAY	0.1US	397		208		397	208	208					
RX_GAIN	N	255		255		255		255					
SAMPLE_MIN	N	4		4		4		4					
SPACE	%US	10		10		10		10					
SPAN	N	63		63		63		63					
SPECTRA	N	46		35		46	28	35					
SSTDODC	O/I	1		1		1		1					
TDA	N	24		64		24	80	64					
WINDOW	O/I	1		1		1		1					
DOPOW COR	O/I	0		0		0		0					

RADAR PARAMETERS

6/2/92

CONTACT: Dave

DATE OF CHANGE: 1551

PARAMETER	UNIT	MODE 1		MODE 2		MODE 3		MODE 4		MODE 5		MODE 6	
		NORM	NEW										
ANT_DIR	CODE	0		0		1		1		2		3	2
ARA	O/I	1		1		1		1		1		1	0
CCP_GAIN	N	6		6		6		6		6		6	
CODE	CODE	0		0		0		0		0		0	
CON_DELTAV	m/s	2.00e0											
DELAY	1/6 μs	300		32		300		32		300		32	35
DODC	O/I	1		1		1		1		1		1	
FILTER	CODE	1		0		1		0		1		0	
GCNUM	N	3		2		3		2		3		2	21
POW_FACTOR	REAL	4.67e-4											
PRP	0.1 μs	2400		1000		2400		1000		2400		1000	1045
PW_BAUD	1/6 μs	40		10		40		10		40		10	
RX_DELAY	0.01 μs	397		208		397		208		397		208	
RX_GAIN	N	255		255		255		255		255		255	
SAMPLE_MIN	N	4		4		4		4		4		4	
SPACE	1/6 μs	10		10		10		10		10		10	
SPAN	N	63		63		63		63		63		63	127
SPECTRA	N	46		35		46		35		26		28	40
SSTDODC	O/I	1		1		1		1		1		1	
TDA	N	24		64		24		64		24		80	60
WINDOW	O/I	1		1		1		1		1		1	0
DOPOWCOR	O/I	0		0		0		0		0		0	

COMMON PARMS	UNIT	NORM	NEW
--------------	------	------	-----

BLANK_TX	1/2 μs	15	
CONSENSUS_SET	N	12	
COOLDOWN	S	0	
FREEDLAY	10 ms	50	
NUMGATES	N	36	
NUMMODES	N	10	
TR_TX	1/2 μs	10	
TX_BLANK	1/6 μs	10	
TX_DUTY	0.1%	50	
TX_TR	1/6 μs	8	

NOTES:

$f_{offs} = 956.9$ $\sigma_{offs} = 354.75$

$$T = \left[\frac{\sigma_{offs} - \sigma_{app}}{20.047} \right]^2$$

Changed window to zero on mode 6.

6/2/92

1551 Z

PARAMETER	UNIT	MODE 7		MODE 8		MODE 9		MODE 10		MODE 11		MODE 12	
		NORM	NEW	NORM	NEW	NORM	NEW	NORM	NEW	NORM	NEW	NORM	NEW
ANT_DIR	CODE	4		4		5	3	5					
ARA	O/I	1		1		1		1					
CCP_GAIN	N	6		6		6		6					
CODE	CODE	0		0		0		0					
CON_DELTA V	m/s	2000		2000		2000		2000					
DELAY	%MS	300		32		300	32	32					
DODC	O/I	1		1		1		1					
FILTER	CODE	1		0		1	0	0					
GCNUM	N	3		2		3	2	2					
POW_FACTOR	REAL	4.67e-4		4.67e-4		4.67e-4		4.67e-4					
PRP	0.1MS	2400		1000		2400	1000	1000					
PW_BAUD	%MS	40		10		40	10	10					
RX_DELAY	0.1MS	397		208		397	208	208					
RX_GAIN	N	255		255		255		255					
SAMPLE_MIN	N	4		4		4		4					
SPACE	%MS	10		10		10		10					
SPAN	N	63		63		63		3					
SPECTRA	N	46		35		46	28	35					
SSTDODC	O/I	1		1		1		1					
TDA	N	24		64		24	80	64					
WINDOW	O/I	1		1		1		1					
DOPOW COR	O/I	0		0		0		0					

RADAR PARAMETERS

940 Z.

CONTACT: *JW*

DATE OF CHANGE: 6/8/92

PARAMETER	UNIT	MODE 1		MODE 2		MODE 3		MODE 4		MODE 5		MODE 6	
		NORM	NEW										
ANT_DIR	CODE	0		0		1		1		2		3	2
ARA	O/I	1		1		1		1		1		1	
CCP_GAIN	N	6		6		6		6		6		6	
CODE	CODE	0		0		0		0		0		0	
CON_DELAY	m/s	2.00e0											
DELAY	1/6 μs	300		32		300		32		300		32	
DODC	O/I	1		1		1		1		1		1	
FILTER	CODE	1		0		1		0		1		0	
GCNUM	N	3		2		3		2		3		2	
POW_FACTOR	REAL	4.67e-4											
PRP	0.1 μs	2400		1000		2400		1000		2400		1000	
PW_BAUD	1/6 μs	40		10		40		10		40		10	
RX_DELAY	0.01 μs	397		208		397		208		397		208	
RX_GAIN	N	255		255		255		255		255		255	
SAMPLE_MIN	N	4		4		4		4		4		4	
SPACE	1/6 μs	10		10		10		10		10		10	
SPAN	N	63		63		63		63		63		63	
SPECTRA	N	46		35		46		35		26		28	
SSTDODC	O/I	1		1		1		1		1		1	
TDA	N	24		64		24		64		24		80	
WINDOW	O/I	1		1		1		1		1		1	
DOPOWCOR	O/I	0		0		0		0		0		0	

COMMON PARAMS	UNIT	NORM	NEW
---------------	------	------	-----

BLANK_TX	1/2 μs	15	
CONSENSUS_SET	N	12	
COOLDOWN	S	0	
FREEDLAY	10 ms	50	
NUMGATES	N	36	
NUMMODES	N	10	
TR_TX	1/2 μs	10	
TX_BLANK	1/6 μs	10	
TX_DUTY	0.1%	50	
TX_TR	1/6 μs	8	

NOTES:

Loss = 96.9

V_{offs} = 354.75

$$T = \left[\frac{V_{offs} - V_{app}}{20.047} \right]^2 - 273.15 \text{ } ^\circ\text{C}$$

Change of mode 6 to be neg, not low
mode 7 & 8 will be Yvert for PASS

Mode 9 is X-15 Low.

6/8/92

940.2

PARAMETER	UNIT	MODE 7		MODE 8		MODE 9		MODE 10		MODE 11		MODE 12	
		NORM	NEW	NORM	NEW	NORM	NEW	NORM	NEW	NORM	NEW	NORM	NEW
ANT_DIR	CODE	4	3	4	5	5	4	5					
ARA	O/I	1		1	0	1		1					
CCP_GAIN	N	6		6		6		6					
CODE	CODE	0		0		0		0					
CON_DELAY	M/S	2000		2000		2000		2000					
DELAY	%US	300		32	35	300	32	32					
DODC	O/I	1		1		1		1					
FILTER	CODE	1		0		1	2	1					
GCNUM	N	3		2	21	3	2	2					
POW_FACTOR	REAL	4.67e4		4.67e4		4.67e4		4.67e4					
PRP	0.1US	2400		1000	1045	2400	1000	1000					
PW_BAUD	%US	40		10		40	10	10					
RX_DELAY	0.1US	397		208		397	208	208					
RX_GAIN	N	255		255		255		255					
SAMPLE_MIN	N	4		4		4		4					
SPACE	%US	10		10		10		10					
SPAN	N	63		3	127	63		63					
SPECTRA	N	46	26	35	40	46	35	35					
SSTDODC	O/I	1		1		1		1					
TDA	N	24		64	60	24	64	64					
WINDOW	O/I	1		1	0	1		1					
DOPOWCOR	O/I	0		0		0		0					

RADAR PARAMETERS

11532

CONTACT: DRW DATE OF CHANGE: 6/8/72

PARAMETER	UNIT	MODE 1		MODE 2		MODE 3		MODE 4		MODE 5		MODE 6	
		NORM	NEW										
ANT_DIR	CODE	0		0		1		1		2	3	3	
ARA	O/I	1		1		1		1		1		1	
CCP_GAIN	N	6		6		6		6		6		6	
CODE	CODE	0		0		0		0		0		0	
CON_DELTAV	m/s	2.00e0											
DELAY	1/6 μs	300		32		300		32		300		32	
DODC	O/I	1		1		1		1		1		1	
FILTER	CODE	1		0		1		0		1		0	
GCNUM	N	3		2		3		2		3		2	
POW_FACTOR	REAL	4.67e-4											
PRP	0.1 μs	2400		1000		2400		1000		2400		1000	
PW_BAUD	1/6 μs	40		10		40		10		40		10	
RX_DELAY	0.01 μs	397		208		397		208		397		208	
RX_GAIN	N	255		255		255		255		255		255	
SAMPLE_MIN	N	4		4		4		4		4		4	
SPACE	1/6 μs	10		10		10		10		10		10	
SPAN	N	63		63		63		63		63		63	
SPECTRA	N	46		35		46		35		26		28	
SSTDODC	O/I	1		1		1		1		1		1	
TDA	N	24		64		24		64		24		80	
WINDOW	O/I	1		1		1		1		1		1	
DOPOWCOR	O/I	0		0		0		0		0		0	

COMMON PARAMS	UNIT	NORM	NEW
---------------	------	------	-----

BLANK_TX	1/2 μs	15	
CONSENSUS_SET	N	12	
COOLDOWN	S	0	
FREEDLAY	10 ms	50	
NUMGATES	N	36	
NUMMODES	N	10	
TR_TX	1/2 μs	10	
TX_BLANK	1/6 μs	10	
TX_DUTY	0.1%	50	
TX_TR	1/6 μs	8	

NOTES:
 $f_{offs} = 956.9$ $v_{offs} = 354.75$
 $T = \left[\frac{v_{offs} - v_{app}}{20.047} \right]^2 - 273.15 \text{ } ^\circ\text{C}$
 Changed modes 5 & 6 to be
 y vert.

1100 (1 0011
 0100

6/18/92

1153Z

PARAMETER	UNIT	MODE 7		MODE 8		MODE 9		MODE 10		MODE 11		MODE 12	
		NORM	NEW	NORM	NEW	NORM	NEW	NORM	NEW	NORM	NEW	NORM	NEW
ANT_DIR	CODE	4	3	4	3	5	4	5					
ARA	O/I	1		1	0	1		1					
CCP_GAIN	A	6		6		6		6					
CODE	CODE	0		0		0		0					
CON_DELTA_V	M/S	2.00e0		2.00e0		2.00e0		2.00e0					
DELAY	%US	300		32	35	300	32	32					
DODC	O/I	1		1		1		1					
FILTER	CODE	1		0		1	0	0					
GCNUM	N	3		2	21	3	2	2					
POW_FACTOR	REAL	4.67e-4		4.67e-4		4.67e-4		4.67e-4					
PRP	0.1US	2400		1000	1045	2400	1000	1000					
PW_BAUD	%US	40		10		40	10	10					
RX_DELAY	.01US	397		208		397	208	208					
RX_GAIN	N	255		355		255		255					
SAMPLE_MIN	N	4		4		4		4					
SPACE	%US	10		10		10		10					
SF_N	N	63		63	127	63		63					
SPECTRA	N	46		35	40	46	35	35					
S_DODC	O/I	1		1		1		1					
SDA	N	24		64	60	24	64	64					
WINDOW	O/I	1		1	0	1		1					
DOPOWCOR	O/I	0		0		0		0					

RADAR PARAMETERS

1216Z

CONTACT: DJW

DATE OF CHANGE: 6/8/92

PARAMETER	UNIT	MODE 1		MODE 2		MODE 3		MODE 4		MODE 5		MODE 6	
		NORM	NEW										
ANT_DIR	CODE	0		0		1		1		2		3	2
ARA	O/I	1		1		1		1		1		1	
CCP_GAIN	N	6		6		6		6		6		6	
CODE	CODE	0		0		0		0		0		0	
CON_DELAY	M/S	2.00e0											
DELAY	1/6 μs	300		32		300		32		300		32	
DODC	O/I	1		1		1		1		1		1	
FILTER	CODE	1		0		1		0		1		0	
GCNUM	N	3		2		3		2		3		2	
POW_FACTOR	REAL	4.67e-4											
PRP	0.1 μs	2400		1000		2400		1000		2400		1000	
PW_BAUD	1/6 μs	40		10		40		10		40		10	
RX_DELAY	0.01 μs	397		208		397		208		397		208	
RX_GAIN	N	255		255		255		255		255		255	
SAMPLE_MIN	N	4		4		4		4		4		4	
SPACE	1/6 μs	10		10		10		10		10		10	
SPAN	N	63		63		63		63		63		63	
SPECTRA	N	46		35		46		35		26		28	
SSTDODC	O/I	1		1		1		1		1		1	
TDA	N	24		64		24		64		24		80	
WINDOW	O/I	1		1		1		1		1		1	
DOPOW_COR	O/I	0		0		0		0		0		0	

COMMON PARAMS

PARAMETER	UNIT	NORM	NEW
BLANK_TX	1/2 μs	15	
CONSELI5_SET	N	12	
COOLDOWN	S	0	
FREEDLAY	10 ms	50	
NUMGATES	N	36	
NUMMODES	N	10	
TR_TX	1/2 μs	10	
TX_BLANK	1/6 μs	10	
TX_DUTY	0.1 %	50	
TX_TR	1/6 μs	8	

NOTES:
 $f_{offs} = 956.9$ $w_{offs} = 354.75$
 $T = \left[\frac{w_{offs} - w_{app}}{20.047} \right]^2 - 273.15 \text{ } ^\circ\text{C}$
 changed modes around

6/8/92

1216Z

PARAMETER	UNIT	MODE 7		MODE 8		MODE 9		MODE 10		MODE 11		MODE 12	
		NORM	NEW	NORM	NEW	NORM	NEW	NORM	NEW	NORM	NEW	NORM	NEW
ANT_DIR	CODE	4		4	5	5	2	5	2				
ARA	O/I	1				1		1	0				
CCP_GAIN	N	6		6		6		6					
CODE	CODE	0				0		0					
CON_DELTAV	M/S	2000		2000		2000		2000					
DELAY	%US	300	32	32		300		32	31				
DODC	O/I	1		1		1		1					
FILTE	CODE	1	0	0		1		0					
GCNUM	N		2	2				2	2				
POW_FACTOR	REAL	4.67e-4		4.67e-4		4.67e-4		4.67e-4					
PRP	0.1US	2400	1000	1000		2400		1000	1045				
PW_BAUD	%US	40	10	10		40		10					
RX_DELAY	0.1US	397	208	208		397		208					
RX_GAIN	N	255		255		255		255					
SAMPLE_MIN	N	4		4		4		4					
SPACE	%US	10		10		10		10					
SPAN	N	63		63		63		63	127				
SPECTRA	N	46	35	35		46		35	40				
SSTDODC	O/I	1		1		1		1					
TDA	N	24	64	64		24		64	60				
WINDOW	O/I	1		1		1		1	0				
DOPOWCOR	O/I	0		0		0		0					

RADAR PARAMETERS

12/17

CONTACT: DATE OF CHANGE: 6/8/92

PARAMETER	UNIT	MODE 1		MODE 2		MODE 3		MODE 4		MODE 5		MODE 6	
		NORM	NEW										
ANT_DIR	CODE	0		0		1		1		2		3	2
ARA	O/I	1		1		1		1		1		1	
CCP_GAIN	N	6		6		6		6		6		6	
CODE	CODE	0		0		0		0		0		0	
CON_DELTAV	m/s	2.00e0											
DELAY	1/6 μs	300		32		300		32		300		32	
DODC	O/I	1		1		1		1		1		1	
FILTER	CODE	1		0		1		0		1		0	
GCNUM	N	3		2		3		2		3		2	
POW_FACTOR	REAL	4.67e-4											
PRP	0.1 μs	2400		1000		2400		1000		2400		1000	
PW_BAUD	1/6 μs	40		10		40		10		40		10	
RX_DELAY	0.01 μs	397		208		397		208		397		208	
RX_GAIN	N	255		255		255		255		255		255	
SAMPLE_MIN	N	4		4		4		4		4		4	
SPACE	1/6 μs	10		10		10		10		10		10	
SPAN	N	63		63		63		63		63		63	
SPECTRA	N	46		35		46		35		26		28	
SSTDODC	O/I	1		1		1		1		1		1	
TDA	N	24		64		24		64		24		80	
WINDOW	O/I	1		1		1		1		1		1	
DOPOWCOR	O/I	0		0		0		0		0		0	

COMMON PARMS

PARAMETER	UNIT	NORM	NEW
BLANK_TX	1/2 μs	15	
CONSENSUS_SET	N	12	
COOLDOWN	S	0	
FREEDLAY	10 ms	50	
NUMGATES	N	36	
NUMMODES	N	10	
TR_TX	1/2 μs	10	
TX_BLANK	1/6 μs	10	
TX_DUTY	0.1%	50	
TX_TR	1/6 μs	8	

NOTES:
 $f_{offs} = 956.9$ $\sigma_{offs} = 354.75$
 $T = \left[\frac{\sigma_{offs} - \sigma_{app}}{20.047} \right]^2 - 273.15$
 Created Dummy mode 11 to turn RASS audio off.

6/8/92
1311 Z

PARAMETER	UNIT	MODE 7		MODE 8		MODE 9		MODE 10		MODE 11		MODE 12	
		NORM	NEW	NORM	NEW	NORM	NEW	NORM	NEW	NORM	NEW	NORM	NEW
ANT_DIR	CODE	4		4	5	5	2	5	2		0		
ARA	O/I	1		1		1		1	0		0		
CCP_GAIN	N	6		6		6		6			6		
CODE	CODE	0		0		0		0			0		
CON_DELTAV	M/S	2000		2000		2000		2000			2000		
DELAY	%US	300	32	32		300		32	35		32		
DOD	O/I	1		1		1		1			0		
FILTER	CODE	1	0	0		1		0			0		
GCNUM	N	3	2	2		3		2	21		6		
POW_FACTOR	REAL	4.67e4		4.67e4		4.67e4		4.67e4			4.67e4		
PRP	O/US	2400	1000	1000		2400		1000	1000		1535		
PW_BAUD	%US	40	10	10		40		10			40		
RX_DELAY	O/US	397	208	208		397		208			208		
RX_GAIN	N	255		255		255		255			255		
SAMPLE_MIN	N	4		4		4		4			4		
SPACE	%US	10		10		10		10			10		
SPAN	N	63		63		63		63	127		63		
SPECTRA	N	46	35	35		46		35	40		1		
SSTDODC	O/I	1		1		1		1			0		
TDA	N	24	64	64		24		64	60		20		
WINDOW	O/I	1		1		1		1	0		1		
DOPOWCOR	O/I	0		0		0		0			0		

RADAR PARAMETERS

1340 Z

CONTACT: *JW*

DATE OF CHANGE: 6/8/92

PARAMETER	UNIT	MODE 1		MODE 2		MODE 3		MODE 4		MODE 5		MODE 6	
		NORM	NEW										
ANT_DIR	CODE	0		0		1		1		2		3	2
ARA	O/I	1		1		1		1		1		1	
CCP_GAIN	N	6		6		6		6		6		6	
CODE	CODE	0		0		0		0		0		0	
CON_DELTA	M/S	2.00e0											
DELAY	1/6 μs	300		32		300		32		300		32	
DODC	O/I	1		1		1		1		1		1	
FILTER	CODE	1		0		1		0		1		0	
GCNUM	N	3		2		3		2		3		2	
POW_FACTOR	REAL	4.67e-4											
PRP	0.1 μs	2400		1000		2400		1000		2400		1000	
PW_BAUD	1/6 μs	40		10		40		10		40		10	
RX_DELAY	0.04 μs	397		208		397		208		397		208	
RX_GAIN	N	255		255		255		255		255		255	
SAMPLE_MIN	N	4		4		4		4		4		4	
SPACE	1/6 μs	10		10		10		10		10		10	
SPAN	N	63		63		63		63		63		63	
SPECTRA	N	46		35		46		35		26		28	
SSTDODC	O/I	1		1		1		1		1		1	
TDA	N	24		64		24		64		24		80	
WINDOW	O/I	1		1		1		1		1		1	
DOPOWCOR	O/I	0		0		0		0		0		0	

COMMON PARMS UNIT NORM NEW

BLANK_TX	1/2 μs	15	
CONSENSUS_SET	N	12	
COOLDOWN	S	0	
FREEDLAY	10 ms	50	
NUMGATES	N	36	
NUMMODES	N	10	
TR_TX	1/2 μs	10	
TX_BLANK	1/6 μs	10	
TX_DUTY	0.1 %	50	
TX_TR	1/6 μs	8	

NOTES:

$f_{doff} = 950.9$ $\nu_{doff} = 354.75$

$T = \left[\frac{\nu_{doff} - 20.047}{20.047} \right]^2 = 273.15$

Created

Moved modes around detelec mode 11

6/8/92

13402

PARAMETER	UNIT	MODE 7		MODE 8		MODE 9		MODE 10		MODE 11		MODE 12	
		NORM	NEW	NORM	NEW	NORM	NEW	NORM	NEW	NORM	NEW	NORM	NEW
ANT_DIR	CODE	4		4	2	5	2	5					
ARA	O/I	1		1		1	0	1					
CCP_GAIN	N	6		6		6		6					
CODE	CODE	0		0		0		0					
CON_DELTAV	M/S	2000		2000		2000		2000					
DELAY	%US	300	32	32	300	300	35	32					
DODC	O/I	1		1		1		1					
FILTER	CODE	1	0	0	1	1	0	0					
GCNUM	N	3	2	2	3	3	21	2					
POW_FACTOR	REAL	4.67e4		4.67e4		4.67e4		4.67e4					
PRP	0.1US	2400	1000	1000	2400	2400	1045	1000					
PW_BAUD	%US	40	10	10	40	40	10	10					
RX_DELAY			208	208	397	397	208	208					
RX_GAIN		2		255		255		255					
SAMPLE_MIN	N	4		4		4		4					
SPACE	%AS	10		10		10		10					
SPAN	N	63		63		63	12.7	63					
SPECTRA	N	46	35	35	46	46	40	35					
SSTDODC	O/I	1		1		1		1					
TDA	N	24	64	64	24	24	60	64					
WINDOW	O/I	1		1		1	0	1					
DOPOWCOR	O/I	0		0		0		0					

RADAR PARAMETERS

1007 Z

CONTACT: *JW*

DATE OF CHANGE: 6/17/92

PARAMETER	UNIT	MODE 1		MODE 2		MODE 3		MODE 4		MODE 5		MODE 6	
		NORM	NEW										
ANT_DIR	CODE	0		0		1		1		2		3	2
ARA	O/I	1		1		1		1		1		1	
CCP_GAIN	N	6		6		6		6		6		6	
CODE	CODE	0		0	1	0		0	1	0		0	1
CON_DELAY	m/s	2.00e0											
DELAY	μs	300		32		300		32		300		32	
DODC	O/I	1		1		1		1		1		1	
FILTER	CODE	1		0		1		0		1		0	
GCNUM	N	3		2		3		2		3		2	
POW_FACTOR	REAL	4.67e-4											
PRP	μs	2400		1000		2400		1000		2400		1000	
PW_BAUD	μs	40		10		40		10		40		10	
RX_DELAY	μs	397		208		397		208		397		208	
RX_GAIN	N	255		255		255		255		255		255	
SAMPLE_MIN	N	4		4		4		4		4		4	
SPACE	μs	10		10		10		10		10		10	
SPAN	N	63		63		63		63		63		63	
SPECTRA	N	46		35		46		35		26		28	
SSTDODC	O/I	1		1		1		1		1		1	
TDA	N	24		64		24		64		24		80	
WINDOW	O/I	1		1		1		1		1		1	
DOPOWCOR	O/I	0		0		0		0		0		0	

COMMON PARMS	UNIT	NORM	NEW
--------------	------	------	-----

NOTES:

$$f = 956.7 \text{ Voffs} = 354.75$$

$$T = \left[\frac{\text{Voffs} - \text{Vapp}}{20.047} \right]$$

Change to 2 bit coding on Low modes.

BLANK_TX	μs	15	
CONSENSUS_SET	N	12	
COOLDOWN	S	0	
FREEDLAY	10ms	50	
NUMGATES	N	36	
NUMMODES	N	10	
TR_TX	μs	10	
TX_BLANK	μs	10	
TX_DUTY	0.1%	50	
TX_TR	μs	8	

6/17/92

1007 Z.

PARAMETER	UNIT	MODE 7		MODE 8		MODE 9		MODE 10		MODE 11		MODE 12	
		NORM	NEW	NORM	NEW	NORM	NEW	NORM	NEW	NORM	NEW	NORM	NEW
ANT_DIR	CODE	4		4	2	5	2	5					
ARA	O/I	1		1		1	0	1					
CCP_GAIN	N	6		6		6		6					
CODE	CODE	0	1	0		0		0	1				
CON_DELTAV	M/S	2000		2000		2000		2000					
DELAY	%US	300	32	32	300	300	35	32					
DODC	O/I	1		1		1		1					
FILTER	CODE	1	0	0	1	1	0	0					
GCNUM	N	3	2	2	3	3	21	2					
POW_FACTOR	REAL	4.67e-4		4.67e-4		4.67e-4		4.67e-4					
PRP	0.1US	2400	1000	1000	2400	2400	1049	1000					
PW_BAUD	%US	40	10	10	40	40	10	10					
RX_DELAY	0.1US	397	208	208	397	397	208	208					
RX_GAIN	N	5		255		255		255					
SAMPLE_MIN	N	-		4		4		1					
SPACE	%US	10		10		10		10					
SPAN	N	63		63		63	127	63					
SPECTRA	N	46	35	35	46	46	40	35					
SSTDODC	O/I	1		1		1		1					
TDA	N	24	64	64	24	24	60	64					
WINDOW	O/I	1		1		1	0	1					
DOPOWCOR	O/I	0		0		0		0					

RADAR PARAMETERS

10532

CONTACT: *JW*

DATE OF CHANGE: *6/18/92*
~~6/18/92~~

PARAMETER	UNIT	MODE 1		MODE 2		MODE 3		MODE 4		MODE 5		MODE 6	
		NORM	NEW										
ANT_DIR	CODE	0		0		1		1		2		3	2
ARA	O/I	1		1		1		1		1		1	
CCP_GAIN	N	6		6		6		6		6		6	
CODE	CODE	0		0		0		0		0		0	
CON_DELAY	M/S	2.00e0											
DELAY	1/6 μs	300		32		300		32		300		32	
DODC	O/I	1		1		1		1		1		1	
FILTER	CODE	1		0		1		0		1		0	
GCNUM	N	3		2		3		2		3		2	
POW_FACTOR	REAL	4.67e-4											
PRP	0.1 μs	2400		1000		2400		1000		2400		1000	
PW_BAUD	1/6 μs	40		10		40		10		40		10	
RX_DELAY	0.01 μs	397		208		397		208		397		208	
RX_GAIN	N	255		255		255		255		255		255	
SAMPLE_MIN	N	4		4		4		4		4		4	
SPACE	1/6 μs	10		10		10		10		10		10	
SPAN	N	63		63		63		63		63		63	
SPECTRA	N	46		35		46		35		26		28	
SSTDODC	O/I	1		1		1		1		1		1	
TDA	N	24		64		24		64		24		80	
WINDOW	O/I	1		1		1		1		1		1	
DOPOWCOR	O/I	0		0		0		0		0		0	

COMMON PARMS	UNIT	NORM	NEW
--------------	------	------	-----

BLANK_TX	1/2 μs	15	
CONSENSUS_SET	N	12	
COOLDOWN	S	0	
FREEDLAY	10 ms	50	
NUMGATES	N	36	
NUMMODES	N	10	
TR_TX	1/2 μs	10	
TX_BLANK	1/6 μs	10	
TX_DUTY	0.1%	50	
TX_TR	1/6 μs	8	

NOTES:
 $f = 956.9$ $V_{offs} = 354.75$
 $T = \left[\frac{V_{offs} - 15_{app}}{20.047} \right]$
 removed pulse coding

6/17/92

1053Z

PARAMETER	UNIT	MODE 7		MODE 8		MODE 9		MODE 10		MODE 11		MODE 12	
		NORM	NEW	NORM	NEW	NORM	NEW	NORM	NEW	NORM	NEW	NORM	NEW
ANT_DIR	CODE	4		4	2	5	2	5					
ARA	O/I	1		1		1	0	1					
CCP_GAIN	N	6		6		6		6					
CODE	CODE	0		0		0		0					
CON_DELTAV	M/S	2000		2000		2000		2000					
DELAY	%US	500	32	32	300	300	35	32					
DODC	O/I	1		1		1		1					
FILTER	CODE	1	0	0	1	1	0	0					
GCNUM	N	3	2	2	3	3	21	2					
POW_FACTOR	REAL	4.67e-4		4.67e-4		4.67e-4		4.67e-4					
PRP	0.1US	2400	1000	1000	2400	2400	1045	1000					
TW_BAUD	%US	40	10	10	40	40	10	10					
TX_DELAY	0.01US	397	208	208	397	397	208	208					
RX_GAIN	N	255		255		255		255					
SAMPLE_MIN	N	4		4		4		4					
SPACE	%US	10		10		10		10					
SPAN	N	63		63		63	127	63					
SPECTRA	N	46		35	46	46	40	35					
SSTDODC	O/I	1		1		1		1					
TDA	N	24	64	64	24	24	60	64					
WINDOW	O/I	1		1		1		1					
DOPOWCOR	O/I	0		0		0		0					